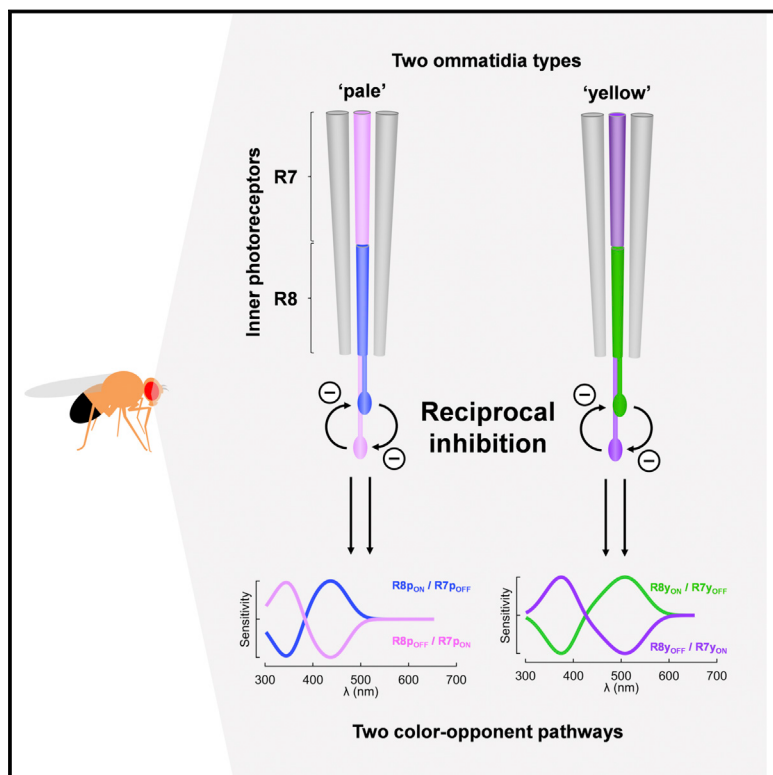


# Color Processing in the Early Visual System of *Drosophila*

## Graphical Abstract



## Authors

Christopher Schnaitmann, Väinö Haikala,  
Eva Abraham, Vitus Oberhauser,  
Thomas Thestrup, Oliver Griesbeck,  
Dierk F. Reiff

## Correspondence

dierk.reiff@biologie.uni-freiburg.de

## In Brief

The *Drosophila* visual system extracts different spectral information at the level of the first synapse, reminiscent of processing in the vertebrate retina.

## Highlights

- Physiological recordings reveal early stages of color opponency
- R7 and R8 photoreceptors of the same type of ommatidia mutually inhibit each other
- HisCl1 histamine receptor mediates direct inhibition between R7 and R8
- Ort histamine receptor is required for feedback inhibition



# Color Processing in the Early Visual System of *Drosophila*

Christopher Schnaitmann,<sup>1</sup> Väinö Haikala,<sup>1</sup> Eva Abraham,<sup>1</sup> Vitus Oberhauser,<sup>1</sup> Thomas Thestrup,<sup>2</sup> Oliver Griesbeck,<sup>2</sup> and Dierk F. Reiff<sup>1,3,\*</sup>

<sup>1</sup>Department for Animal Physiology and Neurobiology, Institute of Biology I, Albert-Ludwigs-University Freiburg, 79104 Freiburg, Germany

<sup>2</sup>Tools for Bio-Imaging, Max Planck Institute of Neurobiology, 82152 Martinsried, Germany

<sup>3</sup>Lead Contact

\*Correspondence: dierk.reiff@biologie.uni-freiburg.de

<https://doi.org/10.1016/j.cell.2017.12.018>

## SUMMARY

Color vision extracts spectral information by comparing signals from photoreceptors with different visual pigments. Such comparisons are encoded by color-opponent neurons that are excited at one wavelength and inhibited at another. Here, we examine the circuit implementation of color-opponent processing in the *Drosophila* visual system by combining two-photon calcium imaging with genetic dissection of visual circuits. We report that color-opponent processing of UV<sub>short</sub>/blue and UV<sub>long</sub>/green is already implemented in R7/R8 inner photoreceptor terminals of “pale” and “yellow” ommatidia, respectively. R7 and R8 photoreceptors of the same type of ommatidia mutually inhibit each other directly via HisCl1 histamine receptors and receive additional feedback inhibition that requires the second histamine receptor Ort. Color-opponent processing at the first visual synapse represents an unexpected commonality between *Drosophila* and vertebrates; however, the differences in the molecular and cellular implementation suggest that the same principles evolved independently.

## INTRODUCTION

Color vision enables animals to distinguish spectral stimuli independent of their relative intensities and provides an extra dimension to vision that facilitates discrimination tasks and intra-specific communication (Gegenfurtner and Kiper, 2003; Kelber et al., 2003). In pollinators such as honeybees, color vision plays a crucial role in flower recognition and, thus, has both ecological and economic importance (Jones and Agrawal, 2017). Color vision requires possession of at least two photoreceptor types with different spectral sensitivities and the ability to compare their outputs. Antagonistic interactions between different channels are a hallmark of sensory processing that enhances stimulus contrast and maximizes information transfer (Dacey and Packer, 2003; Olsen and Wilson, 2008; Clarke et al., 2015). In color vision, this opponency between spectral channels solves the critical shortcoming that any single photore-

ceptor cannot distinguish between changes in brightness and spectral information (Rushton, 1972; Dacey and Packer, 2003; Gegenfurtner and Kiper, 2003).

Much of our knowledge of color-opponent processing is based on vertebrates. In humans and other trichromatic primates, the signals of short (S), middle (M), and long (L) wavelength-sensitive cone photoreceptors are combined antagonistically to create two spectrally opponent pathways. In the first pathway, L and M cone signals mutually inhibit each other. In the second pathway S cone signals and the summed signals of L and M cones mutually inhibit each other (Gegenfurtner and Kiper, 2003; Dacey and Packer, 2003; Demb and Singer, 2015). These color opponencies correspond with the red-green and blue-yellow opponent axes of human and macaque color perception and are implemented at the first visual synapse (Abramov and Gordon, 1994; Dacey and Packer, 2003). Different types of cones converge onto horizontal cells, and the latter establish reciprocal sign-inverting synapses with cone terminals (Dacey and Packer, 2003; Wässle, 2004; Demb and Singer, 2015). This circuit adapts photoreceptor output to the intensity of ambient light, enhances achromatic and chromatic image contrast, and renders the terminals of vertebrate cones color-opponent. Furthermore, it provides the basis for the center-surround organization of cone terminals and bipolar cells. However, the exact biophysical mechanisms that underlie this critical processing stage in the retina are still unresolved (Chapot et al., 2017).

Compared with the vertebrate retina, we know much less about color-opponent processing in insects. Color-opponent neurons have been recorded in a few species, but the lack of genetic amenability prohibited identification of the underlying circuits and synaptic mechanisms (Kien and Menzel, 1977; Paulk et al., 2009; Behnia and Desplan, 2015). Recent studies of sensory processing in *Drosophila* suggest that such insights may be revealed in this model organism (Olsen and Wilson, 2008; Behnia and Desplan, 2015); however, color-opponent neurons have not been previously identified. Such neurons are expected because fruit flies exhibit a multitude of wavelength-dependent behaviors, including phototaxis, spectral preference, and color memory (Heisenberg and Buchner, 1977; Gao et al., 2008; Yamaguchi et al., 2010; Schnaitmann et al., 2013; Karuppudurai et al., 2014; Melnattur et al., 2014). Moreover, *Drosophila* is a classic model for studies of visual system development and connectivity and offers almost unlimited genetic amenability (Wernet



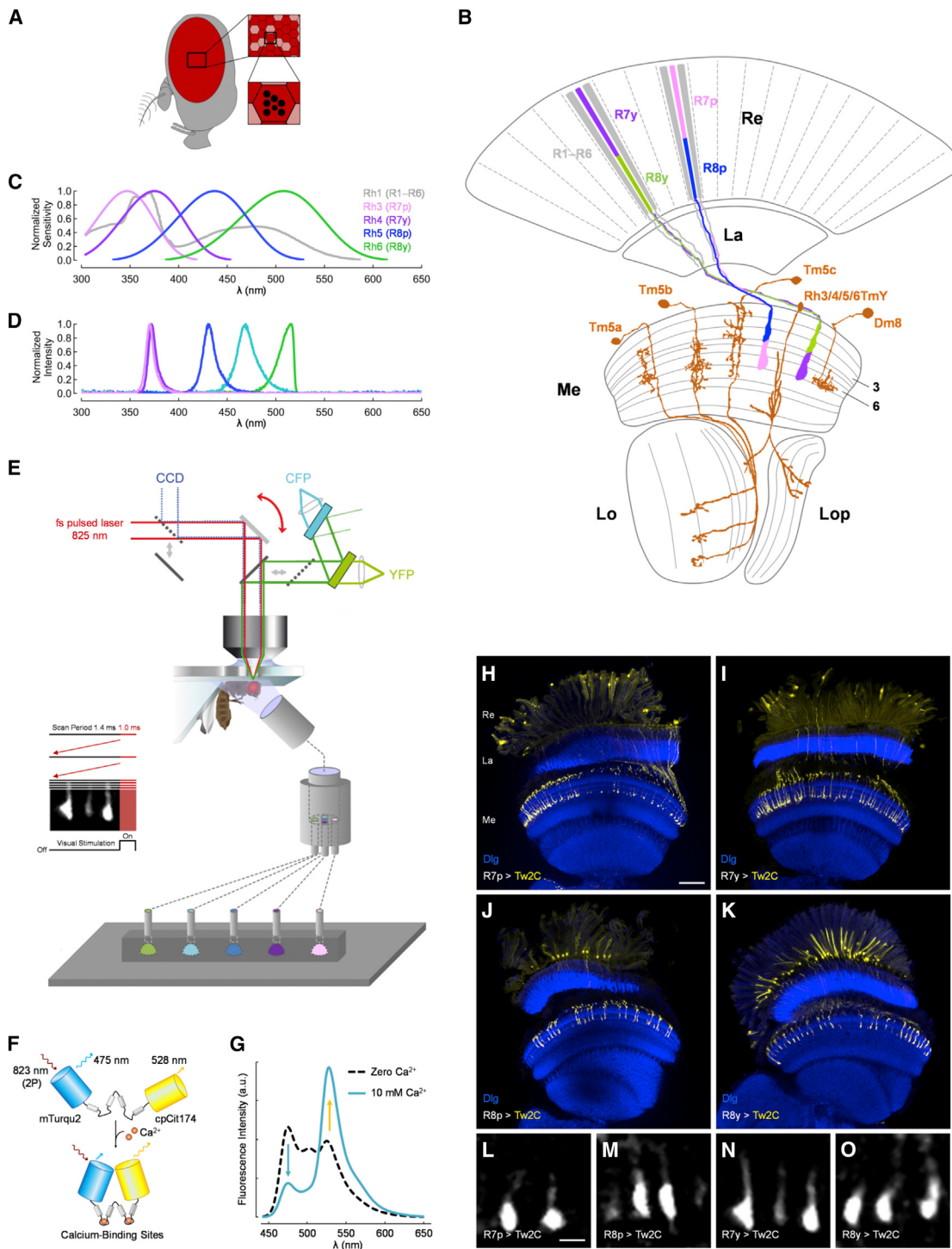


**Figure 1. Schematic of the *Drosophila* Visual System and Experimental Setup**

(A) Compound eye of *Drosophila* with ~800 ommatidia of either the p (rose, 30%) or y (red, 70%) subtype (ignoring the specialized dorsal rim region). Each ommatidium contains six outer photoreceptors, R1–R6, and a superimposed pair of inner photoreceptors, R7/R8.

(B) R7 and R8 axons project from the retina (Re) to the medulla (Me), where they terminate in layer six and layer three, respectively; R1–R6 axons terminate in the lamina (La). Rhodopsin (*rh*) expression in R7/R8 photoreceptors differentiates p and y ommatidia. R7/R8 cells express *rh3/rh5* in p (light purple/blue) and *rh4/rh6* in y (dark purple/green) ommatidia, respectively. R1–R6 cells homogeneously express *rh1* (gray). Candidate color-opponent neurons postsynaptic to R7/R8 cells are depicted in orange.

(legend continued on next page)

et al., 2006; Takemura et al., 2011). In the *Drosophila* eye, each ommatidium houses six outer photoreceptors, R1–R6, and a pair of superimposed inner photoreceptors, R7/R8 (Figure 1A) that release histamine as neurotransmitter (Hardie, 1989). The broadband-sensitive R1–R6 photoreceptors express *rhodopsin 1* (*rh1*), project to the lamina (Figures 1B and 1C), and provide the major input to the motion vision system (Heisenberg and Buchner, 1977; Salcedo et al., 1999; Yamaguchi et al., 2008). Although not required for color vision, R1–R6 photoreceptors were recently shown to also contribute to it (Schnaitmann et al., 2013). In R7/R8 photoreceptor pairs, precise genetic control of *rhodopsin* expression determines the two major types of ommatidia, “pale” (p) and “yellow” (y), that are stochastically distributed over the main part of the eye (Figures 1A–1C; Wernet et al., 2006). R7p and R8p photoreceptors express *rh3* with maximum sensitivity in the short-UV and *rh5* with maximum sensitivity in the blue spectral range, respectively. R7y and R8y photoreceptors express *rh4* with maximum sensitivity in the long-UV and *rh6* with maximum sensitivity in the green spectral range, respectively (Figure 1C; Salcedo et al., 1999). These four types of inner photoreceptors provide the major input to the color vision system in the medulla (Figure 1B), to which they project without making chemical synapses in the lamina (Heisenberg and Buchner, 1977; Yamaguchi et al., 2010; Schnaitmann et al., 2013).

Direct investigation of color-opponent processing using electrophysiological recordings has so far proved elusive by the technical difficulties associated with the stacked arrangement of the R7 and R8 cells and their postsynaptic partners in *Drosophila* (Behnia and Desplan, 2015; Kelber, 2016; but see Weir et al., 2016). However, behavioral studies on *Lucilia* and *Drosophila* suggest that flies compare the signals of R7 and R8 photoreceptors of the same type of ommatidia (p and y) to distinguish color (Troje, 1993; Schnaitmann et al., 2013). Intracellular recordings from distal segments of photoreceptors in large dipteran flies and most other insect species revealed no sign of spectral inhibition; therefore, this comparison is thought to be implemented downstream of *Drosophila* inner photoreceptors (Hardie, 1977; Smola and Meffert, 1979; Horridge et al., 1983; Matic, 1983; Menzel et al., 1986; Peitsch et al., 1992; Qiu and Arikawa, 2003; Arikawa et al., 2005; Skorupski and Chittka, 2010; Chen et al., 2013; Schmeling et al., 2014). Candidate color-opponent neurons postsynaptic to inner photoreceptors have been revealed in behavioral, genetic, and anatomical studies in

*Drosophila* and include Tm9, Tm20, Tm5a/b/c, and certain TmY cells (Figure 1B; Gao et al., 2008; Karuppudurai et al., 2014; Melnattur et al., 2014; Jagadish et al., 2014). However, these studies do not exclude the possibility of color-opponent processing at the level of photoreceptors. For example, intracellular recordings in a few butterfly species revealed excitatory and inhibitory response components in particular photoreceptors (Horridge et al., 1983; Matic, 1983; Chen et al., 2013). Finally, the responses of photoreceptor terminals have not been recorded in any insect species so far. This leaves open the question of whether local inhibitory circuit mechanisms render photoreceptor output color-opponent and, if so, how these mechanisms compare with processing in the vertebrate retina.

Here we report physiological recordings from inner photoreceptor terminals of *Drosophila*, combining two-photon calcium imaging, spectral stimulation, and use of the fluorescent genetically encoded calcium reporter Twitch-2C. Presynaptic UV<sub>short</sub>/blue and UV<sub>long</sub>/green color opponencies are evident in the terminals of the inner photoreceptors R7/R8 of p and y ommatidia. Genetic dissection of the peripheral visual circuits enabled identification of the photoreceptor interactions underlying color-opponent processing: R7 and R8 photoreceptors of the same type of ommatidia mutually inhibit each other at the level of their presynaptic terminals, whereas R1–R6 do not contribute to spectrally opponent processing in R7/R8 photoreceptor terminals. Two concurrent circuit mechanisms that involve the distinct histamine receptors HisCl1 and Ort mediate this processing. Direct inhibitory synaptic interactions between the terminals of R7/R8 pairs are mediated by HisCl1, and feedback inhibition with similar spectral tuning requires expression of Ort. These results illustrate that the *Drosophila* visual system subtracts different spectral channels at the first synapse, reminiscent of processing in the vertebrate retina, albeit by entirely different synaptic and cellular mechanisms.

## RESULTS

### Physiological Analysis and Spectral Sensitivity of *Drosophila* Photoreceptor Terminals

We recorded the activity of R7 and R8 photoreceptor terminals *in vivo* using functional two-photon calcium imaging (Figure 1E) and the genetically encoded ratiometric fluorescent calcium reporter Twitch-2C (Thestrup et al., 2014; Figures 1F and 1G). Twitch-2C was expressed in individual types of inner

(C) Spectral sensitivity of Rhodopsins expressed in the five photoreceptor types of the eye (color-coded as in B). Maximum sensitivities: 478 nm (Rh1), 345 nm (Rh3), 375 nm (Rh4), 437 nm (Rh5), and 508 nm (Rh6). An accessory pigment mediates additional UV sensitivity of R1–R6. Data based on Salcedo et al. (1999).

(D) Emission spectra of visual stimuli (STAR Methods).

(E) Experimental configuration. Light from five LEDs was combined into a single fiber and presented to the frontal part of the eye. The two fluorophores of Twitch-2C (see F) were simultaneously recorded in photoreceptor terminals using two-photon laser-scanning microscopy (ratiometric imaging). Activation of LEDs and fluorescence recording were separated in time using fly back stimulation (schematic modified from Reiff et al. (2010); STAR Methods).

(F) Schematic representation of the genetically encoded fluorescent calcium reporter Twitch-2C (Thestrup et al., 2014). Binding of calcium mediates a conformational change that alters fluorescence resonance energy transfer between mTurquoise2 and cpCitrine174, resulting in a change in the intensity ratio of blue and yellow fluorescence.

(G) Emission spectra of Twitch-2C at zero (dashed line) and saturated (solid line) calcium.

(H–K) Cell-specific expression of Twitch-2C in (H) R7p, (I) R7y, (J) R8p, and (K) R8y inner photoreceptor types (*rhodopsin* promoter::LexA > LexAop-Twitch-2C; see also Table S1). Shown are confocal images of optic lobes and immunostaining of neuropil (anti-Dlg, blue) and Twitch-2C (anti-GFP, yellow). Scale bar, 45 μm.

(L–O) Twitch-2C-expressing terminals of (L) R7p, (M) R8p, (N) R7y, and (O) R8y inner photoreceptors in typical recording situations. Scale bar, 5 μm.

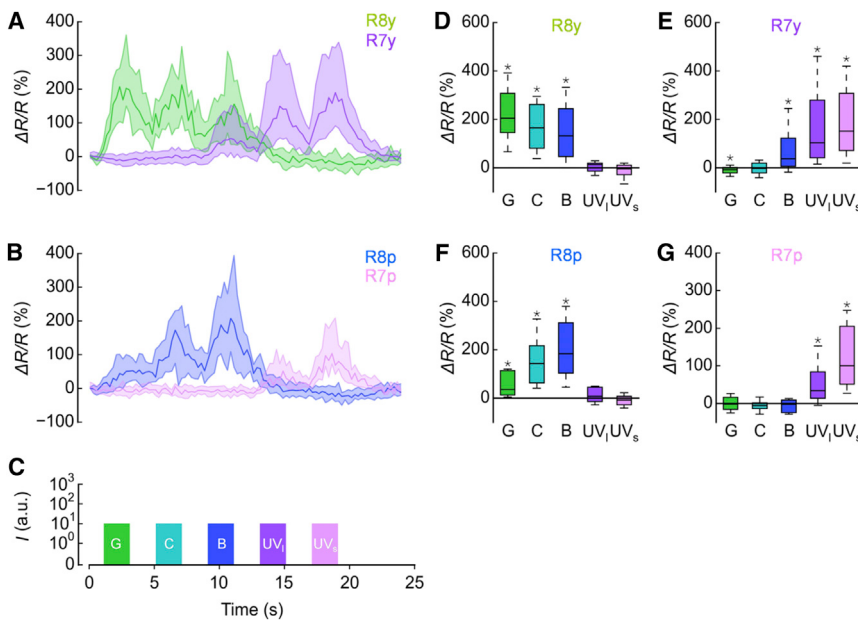


**Figure 2. Spectral Tuning of Inner Photoreceptor Terminals**

(A and B) Time course of fluorescence changes ( $\Delta R/R$ ) in (A) R8y/R8y and (B) R7p/R8p terminals expressing Twitch-2C during presentation of monochromatic visual stimuli (C). Data are represented as median (solid line) and 25%/75% quantiles (shading).

(C) Monochromatic visual stimuli (G, green; C, cyan; B, blue; UV, long UV; UV<sub>s</sub>, short UV, intensity  $10^1$  a.u.).

(D–G) Maximum responses of (D) R8y, (E) R7y, (F) R8p, and (G) R7p inner photoreceptor terminals to monochromatic stimuli in the experiments in (A) and (B). Data are represented as median (solid line), 10%/90% quantiles (whiskers), and 25%/75% quantiles (box). Asterisks indicate responses significantly different from the fluorescence ratio at rest, R<sub>0</sub> ( $p < 0.05$ , Wilcoxon test).

For genotypes, n recordings, see Table S1. See also Figure S1.

photoreceptors using newly generated *UAS-twitch-2C*, *LexAop-twitch-2C*, and cell-specific *rhodopsin* promoter LexA-driver lines as well as existing *rhodopsin* promoter GAL4-driver lines (Figures 1H–1O; STAR Methods). The eyes of flies were stimulated using five different light-emitting diodes (LEDs) with maximum emission close to the absorption maxima of the five Rhodopsin variants expressed in the compound eye (Salcedo et al., 1999; Figures 1C and 1D). The contamination of the recorded Twitch-2C fluorescence signals by photons from the visual stimuli was prevented using fly back stimulation (Figure 1E; STAR Methods; Reiff et al., 2010).

In our first experiments, we characterized the physiological responses of inner photoreceptor terminals in flies with intact retinal circuits (Figure 2). A sequence of five different monochromatic stimuli elicited unique activity patterns in each type of terminal. Wavelengths close to the absorption maxima of the expressed Rhodopsin (Figures 1C and 1D) elicited the largest responses (Figure 2). R7/R8 terminals of the same type of ommatidia (p and y) exhibited complementary wavelength sensitivity with small inhibitory responses to green light in R7y terminals (Figures 2A–2C; quantification in Figures 2D–2G). Terminals of other photoreceptor types did not exhibit observable spectral inhibition (Figure 2). The observed spectral sensitivity profiles were largely intensity-independent (tested over four orders of magnitude; Figures S1I–S1L), suggesting that the calcium reporter Twitch-2C, photoreceptors, and terminals were not saturated under any of the stimulus conditions.

We hypothesized that weak spectral inhibition in R7y terminals and the failure to detect spectral inhibition in other types of terminals could be associated with a low concentration of intracellular calcium in dark-adapted photoreceptor terminals and the non-linearity of Twitch-2C (Thestrup et al., 2014). If so, visual stimuli that shift presynaptic calcium into the dynamic range of the calcium reporter should unmask spectral inhibition. We tested this hypothesis by stimulating flies with composite stimuli

that included a mix of the preferred wavelength of the recorded photoreceptor plus individual other wavelengths (Figures 3; STAR Methods). The individual additional wavelengths were presented with increased intensity to facilitate the detection of potential spectral inhibition. Intensities comparable with the intensities of composite stimuli did not saturate photoreceptor responses (Figures S1 and 3). Compared with the responses to preferred monochromatic light, composite stimuli should elicit increased responses in the absence and decreased responses in the presence of spectral inhibition. We found a unique response profile for each type of terminal with distinct additive (ON) and subtractive (OFF) wavelength ranges (Figures 3E–3H). Composite stimuli elicited increased responses whenever the additional wavelength elicited excitation in the recorded type of terminal in the experiments shown in Figure 2 and reduced responses when the additional wavelength did not excite the recorded type of terminal (Figure 2). UV stimuli inhibited green-sensitive R8y terminals; green and cyan stimuli inhibited UV<sub>long</sub>-sensitive R7y terminals; UV stimuli inhibited blue-sensitive R8p terminals; and green, cyan, and blue stimuli inhibited UV<sub>short</sub>-sensitive R7p terminals (Figures 3E–3H). Notably, composite stimuli also elicited significant inhibition at intensity ratios as low as 1:1 and 1:3 (preferred: inhibitory wavelength), depending on the type of photoreceptor (Figures S1M–S1P). In summary, R7 and R8 terminals processed stimulus mixtures either additively or by color-opponent processing (Figure 3).

### Interacting Photoreceptors

Because spectral inhibition is mediated by interactions between different types of photoreceptors, it should be eliminated in flies with only a single functional type of photoreceptor. We tested this using *norpA* mutant flies with *norpA* rescue in a single type of photoreceptor (Schnaitmann et al., 2013) that co-expressed Twitch-2C (STAR Methods). The *norpA* mutation disrupts phospholipase C function (light-induced activation of

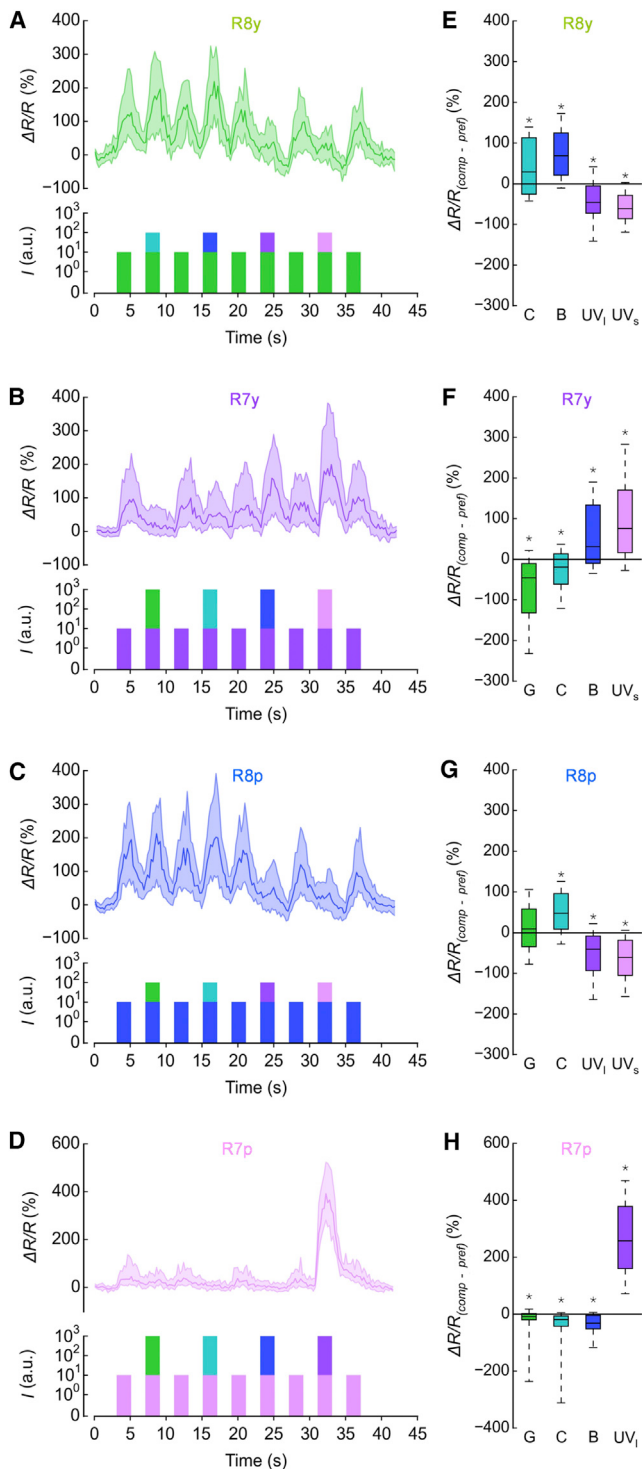


**Figure 3. Responses of R7/R8 Terminals to Spectrally Composite Stimuli Reveal Additive and Subtractive Processing**

(A–D) Time course of fluorescence changes during alternating presentation of preferred monochromatic stimuli and spectrally composite stimuli in (A) R8y, (B) R7y, (C) R8p, and (D) R7p photoreceptor terminals (stimulus protocols are shown below the recording traces). Composite stimuli contained two wavelengths, the preferred one and one of the other wavelengths.

phosphoinositide signaling) and renders photoreceptors insensitive to light (*norpA*; Inoue et al., 1985). Monochromatic stimuli ( $10^3$  a.u., resembling the intensity of composite stimuli) elicited responses over an extended spectral range and with increased amplitude in photoreceptor terminals of *norpA* mutant flies compared with flies with unperturbed photoreceptor function (R7y; Figure 4A; R7p, R8y, and R8p; Figures S3A, S4A, and S5A). Most importantly, spectral inhibition was absent in all types of photoreceptors that now exhibited additive processing of particular composite stimuli (the same stimuli as shown in Figure 3) (R7y; Figure 4B; R7p, R8y, and R8p; Figures S3B, S4B, and S5B). Furthermore, spectral inhibition was similarly absent in all types of terminals at different intensity ratios (Figures S1M–S1P, gray lines). Thus, different types of functional photoreceptors are required for the generation of color-opponent responses in R7/R8 terminals.

To identify photoreceptors that detect the inhibitory wavelength and convey inhibition to other photoreceptors, we analyzed terminals of *norpA* mutant flies with *norpA* rescue in different pairwise combinations of photoreceptor types (including inner R7/R8 and outer R1–R6; STAR Methods). R7y terminals were inhibited by green and cyan light that excites R8y and R8p but not R7p photoreceptors (Figure 3). Thus, we rescued *norpA* in R7y/R8y and R7y/R8p but not in R7y/R7p photoreceptors. The same rationale was used for the analysis of R7p, R8y, and R8p. Functional rescue of R7y/R8y photoreceptors restored spectral tuning and color opponency in R7y terminals (Figures 4C–4F), whereas *norpA* rescue in R7y/R8p cells failed (Figures S2A and S2B). R7p terminals received antagonistic input only when *norpA* was rescued in R7p/R8p, whereas *norpA* rescue in R7p/R8y cells failed (Figures S3C–S3F). In R8y (Figures S4C–S4F) and R8p (Figures S5C–S5F) terminals, only *norpA* rescue in R8y/R7y and in R8p/R7p cells, respectively, restored spectrally antagonistic processing. These results are summarized in Figure 4G.

Outer photoreceptors have recently been shown to contribute to *Drosophila* color vision (Schnaitmann et al., 2013). In the experiments described above, R1–R6 cells were light-insensitive and were therefore not required for color-opponent processing in R7/R8 terminals. We further analyzed the role of R1–R6 photoreceptors by combining *norpA* rescue in R1–R6 with *norpA* rescue in R7y, R7p, R8p, or R8y cells (STAR Methods). Additional *norpA* rescue in R1–R6 cells did not restore spectral tuning and color opponency in any of the R7/R8 terminals (Figures S2C and S2D, S3G and S3H, S4G and S4H, and S5G and S5H). Finally, we studied flies with triple *norpA* rescue (STAR Methods) in R7y/R8y/R1–R6 cells (Figures S2E and S2F). The R7y terminals of these flies exhibited spectral tuning and color opponency comparable with flies with functional phototransduction in exclusively R7y/R8y (Figures 4C–4G) or flies with unperturbed retinal

(E–H) Comparison of responses to preferred monochromatic and composite stimuli ( $\Delta R/R_{comp} - \Delta R/R_{pref}$ ) in the experiments shown in (A)–(D). Additive and subtractive (opponent) processing of the two wavelengths of composite stimuli is indicated by positive and negative values, respectively, in (E) R8y, (F) R7y, (G) R8p, and (H) R7p.

The recording traces and boxplots are as in Figure 2; for n recordings, see Table S1. Asterisks indicate significant inhibition or additional excitation ( $p < 0.05$ , Wilcoxon test). See also Figure S1.

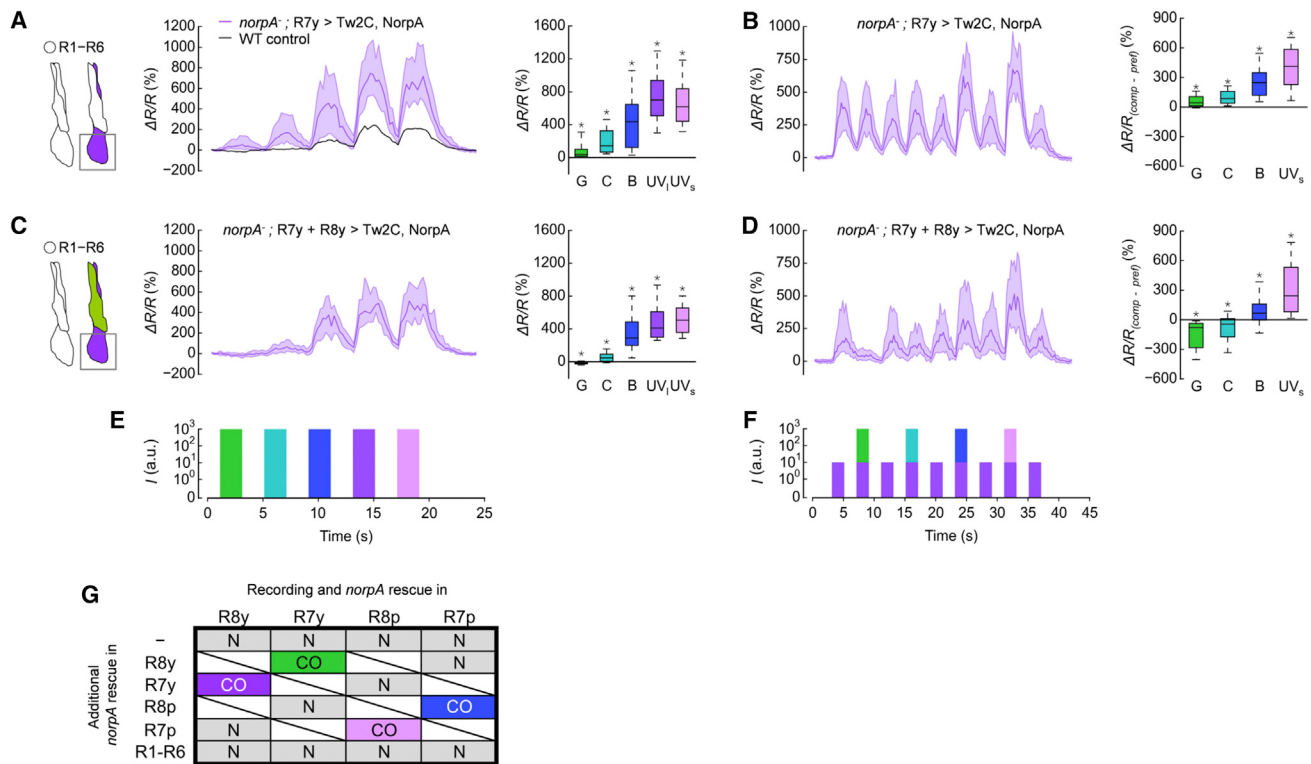


**Figure 4. Color Opponency and Spectral Tuning of Inner Photoreceptor Terminals Are Mediated by Reciprocal Inhibitory Interactions between R7/R8 of the Same Type of Ommatidia**

(A) Time course of fluorescence changes (purple trace) and maximum responses (boxplots) of R7y terminals to monochromatic stimuli (intensity  $10^3$  a.u., see [E]) in flies with light sensitivity in exclusively R7y photoreceptors (*norpA* mutant with *norpA* rescue in R7y; Table S1). The R7y terminals in these flies were excited by green light ( $p < 0.05$ , Wilcoxon test), whereas the R7y terminals in control flies were inhibited (black trace,  $p < 0.05$ , Wilcoxon test; see also Figure S1J).

(B) Time course of fluorescence changes and comparison of responses to preferred monochromatic ( $UV_{long}$ ) and composite stimuli in R7y terminals in the same flies as shown in (A). R7y terminals did not exhibit spectral inhibition and processed  $UV_{long}$  and green light (or cyan) additively ( $p < 0.05$ , Wilcoxon test; compare with control flies in Figures 3B and 3F).

(C) The same experiment as in (A) but with *norpA* rescue in R7y and R8y photoreceptors (Table S1). In the R7y terminals of these flies, spectral tuning and inhibition by green light were restored ( $p < 0.05$ , Wilcoxon test, compare with [A]).

(D) The same experiment as in (B) but with *norpA* rescue in R7y and R8y photoreceptors. Spectral inhibition by green and cyan light was restored ( $p < 0.05$ , Wilcoxon test, compare with (B) and control flies in Figures 3B and 3F).

(A–D) The same type of plots as in Figures 2 and 3; for n recordings, see Table S1. Asterisks indicate significant difference from  $R_0$  (A and C) and significant inhibition or additional excitation (B and D) ( $p < 0.05$ , Wilcoxon test). In the schemes at the left, functional and non-functional photoreceptors are depicted in color and in white, respectively.

(E) The stimuli used in (A) and (C).

(F) The stimuli used in (B) and (D).

(G) Summary of the complete set of imaging experiments with *norpA* rescue in single inner photoreceptor types and different pairwise combinations of photoreceptor types, including R1-R6 cells (CO, color opponency; N, absence of color opponency).

See also Figures S2, S3, S4, and S5.

circuits (Figures 3B and S1J). Qualitatively similar results were observed in the terminals of R7p, R8p, or R8y in flies with triple *norpA* rescue in R7p/R8p/R1-R6 or R7y/R8y/R1-R6 (Figures S3I and S3J, S4I and S4J, and S5I and S5J). Thus, we found no evidence for a contribution of R1-R6 to color-opponent processing in R7/R8 photoreceptor terminals (Figure 4G).

In summary, color-opponent processing in *Drosophila* inner photoreceptor terminals is based on mutual inhibitory interactions between R7 and R8 cells of the same ommatidial type. Spectral excitation (ON) of the terminals of a certain type of inner photoreceptor is antagonized (OFF) by simultaneous spectral excitation of its genetically determined partner photoreceptor.

This fundamental processing underlies p and y color opponencies in R7/R8 terminals: R7p/R8p ( $UV_{short}$ -ON/blue-OFF), R8p/R7p (blue-ON/ $UV_{short}$ -OFF), R7y/R8y ( $UV_{long}$ -ON/green-OFF), and R8y/R7y (green-ON/ $UV_{long}$ -OFF).

### R7 and R8 Are Synaptically Connected and Express the Histamine Receptor HisCl1

Interacting R7p/R8p and R7y/R8y cells might belong to the same ommatidium or different ommatidia of the same type. They might furthermore interact directly or indirectly via unknown interneurons (Figure 5A). We used GFP reconstitution across synaptic partners (GRASP) (Gordon and Scott, 2009) to test

whether R7/R8 cells of the same ommatidium interact with each other directly (Figure 5B). Expression of complementary GFP subunits in R7 and R8 of either p or y ommatidia revealed puncta of GFP fluorescence in layers M1–M3 of the medulla (Figures 5C–5D'), where the terminals of R7 and R8 co-ramify and interdigitate (Figure 5E). These GRASP signals likely indicate chemical synapses, as supported by few chemical synapses between R7 and R8 terminals that were described in a prior serial electron microscopy (EM) analysis (Takemura et al., 2013).

Given that arthropod photoreceptors release histamine as a neurotransmitter (Hardie, 1989), direct synaptic interactions might be mediated by the inhibitory histamine-gated chloride channels Ort and HisCl1 (Witte et al., 2002; Pantazis et al., 2008). Ort has a major function in the visual system of *Drosophila* and is required for various visual behaviors (Gao et al., 2008). Its expression in the optic lobe is restricted to neurons postsynaptic to R1–R6 and R7/R8 cells in the lamina and medulla, respectively (Witte et al., 2002; Gao et al., 2008; Pantazis et al., 2008; Karuppudurai et al., 2014; Jagadish et al., 2014). We found strong *ort* promoter activity in the lamina and medulla and no expression in R7/R8 photoreceptors of the retina (Figure 5F). These findings are in accordance with the work of Gao et al. (2008) and recent results from deep sequencing in pupae (Tan et al., 2015; Figure 5I). Thus, Ort is very unlikely to mediate direct R7/R8 interactions.

In the visual system, the second *Drosophila* histamine receptor, HisCl1, has been reported to be expressed exclusively in lamina glia cells (Pantazis et al., 2008), and mutations in *hisCl1* cause only minor visual defects (Gao et al., 2008; Pantazis et al., 2008). In our experiments, *hisCl1*-GAL4 (Pantazis et al., 2008) drove very weak expression of mCD8::GFP in R7/R8 (data not shown). We followed up this unexpected result using *hisCl1*::GFP<sup>TRG.105</sup> flies that carry a fosmid-based GFP-tagged *hisCl1* gene (FlyFos020750; Sarov et al., 2016). Because fosmids include most of the regulatory sequences, HisCl1::GFP expression should recapitulate the expression of endogenous unlabeled HisCl1 and allow subcellular localization (Sarov et al., 2016). HisCl1::GFP was expressed strongly in the lamina but also in the medulla in inner photoreceptor terminals that co-expressed DsRed (Figures 5G and 5H). Confocal microscopy revealed distinct puncta of GFP fluorescence restricted to medulla layers M1–M3 (Figure 5H), comparable with the localization of the GRASP signals (Figures 5C–5D'). Two fosmid-based, GFP-tagged, muscle-specific genes (STAR Methods) were used as controls. These fosmids similarly labeled R7/R8 with DsRed, whereas GFP was not expressed in the visual system (data not shown). Expression of HisCl1 in R7/R8 is furthermore supported by expression profiling in pupae (Figure 5I; Tan et al., 2015). In summary, the genetic and anatomical studies strongly suggest that spectral inhibition involves direct inhibitory interactions between R7/R8 terminals of the same ommatidium that are mediated by the histamine receptor HisCl1.

## Two Parallel Circuit Mechanisms Mediate Color Opponency and Involve Distinct Histamine Receptors

We investigated photoreceptor terminals in *ort*, *hisCl1*, and *ort/hisCl1* mutants to investigate the role of Ort and HisCl1 in color opponency in R7/R8 terminals (Figures 6 and S6). Responses to monochromatic and composite stimuli showed that *ort* and

*hisCl1* are differentially required in R7 and R8 cells. The R8y terminals in these mutants uniformly exhibited increased excitatory responses to UV<sub>long</sub> stimuli (Figure 6A; Figure S6A), and addition of UV<sub>long</sub> to green stimuli revealed additive processing instead of spectral inhibition (Figures 6E and S6E). R7y terminals in *ort* and *hisCl1* mutant flies showed unaltered inhibitory responses to green light and spectral inhibition to composite stimuli (UV<sub>long</sub> plus green). In contrast, R7y terminals in *ort/hisCl1* double mutants were excited by green light (Figures 6B and S6B), and composite stimuli failed to elicit spectral inhibition (Figures 6F and S6F). Qualitatively similar results were found in R8p and R7p terminals. R8p terminals in all mutants uniformly exhibited increased excitatory responses to UV<sub>short</sub> (Figures 6C and S6C), and addition of UV<sub>short</sub> to blue stimuli failed to elicit spectral inhibition (Figures 6G and S6G). In R7p, only terminals of *ort/hisCl1* double mutants were excited by blue light (Figures 6D and S6D), and composite stimuli (UV<sub>short</sub> plus blue) failed to elicit spectral inhibition (Figures 6H and S6H). In summary, expression of either Ort or HisCl1 is sufficient to generate color opponency in R7p/y terminals, whereas both histamine receptors are required simultaneously for color opponency in R8p/y terminals.

In the mutant studies above, expression of functional histamine receptors was prohibited in the entire organism. To test whether *hisCl1* is specifically required in inner photoreceptors, we suppressed *hisCl1* expression in R8p or R8y cells using *UAS-hisCl1* RNAi (Oh et al., 2013). Expression of *hisCl1* RNAi in R8p or R8y cells caused defects in spectral processing, similar to the defects in *hisCl1* mutants (Figure S7). Thus, expression of *hisCl1* in R8 cells is required for color opponency in R8 terminals. R7 cells were excluded from this analysis because of intact color-opponent processing in *hisCl1* mutants (Figures 6B, 6D, 6F, and 6H).

Finally, we generated *UAS-hisCl1* transgenic flies (STAR Methods) and tested whether *hisCl1* expression exclusive in the recorded type of photoreceptor is sufficient for color-opponent processing in their terminals (Figures 7 and S8). We verified GAL4-driven expression of *UAS-hisCl1* by RT-PCR (Figure S8). Because of the differential requirement of both histamine receptors for color-opponent processing in R7 and R8 terminals, we restored *hisCl1* expression in R8 in *hisCl1* mutant flies and in R7 in *ort/hisCl1* double-mutant flies (*hisCl1* rescue flies). As negative controls we used flies with the respective histamine receptor mutant background with *UAS-hisCl1* but no GAL4 driver (*rhodopsin-LexA*-driven *LexAop-twitch-2C* expression). Flies with intact *ort* and *hisCl1* expression served as positive controls.

R7y/p and R8p terminals of *hisCl1* rescue flies and of positive control flies exhibited similar responses to the most efficient opponent wavelength (R7y, green; R7p, blue; R8p, UV<sub>short</sub>). In contrast, R7y/p and R8p terminals of negative control flies lacking *hisCl1* (similar to the *hisCl1* mutant flies shown in Figure 6) exhibited increased excitatory responses to the same stimuli (Figures 7B–7D and S8B–S8D). Thus, targeted expression of *hisCl1* restored the responses to monochromatic stimuli in R7y/p and R8p photoreceptors terminals of *hisCl1* mutant flies. R8y terminals of negative controls (Figures 7A and S8A), however, did not exhibit increased responses to UV<sub>long</sub> as in *hisCl1* mutants (Figure 6) and showed the same responses as positive and negative controls. Most importantly, composite stimuli (the

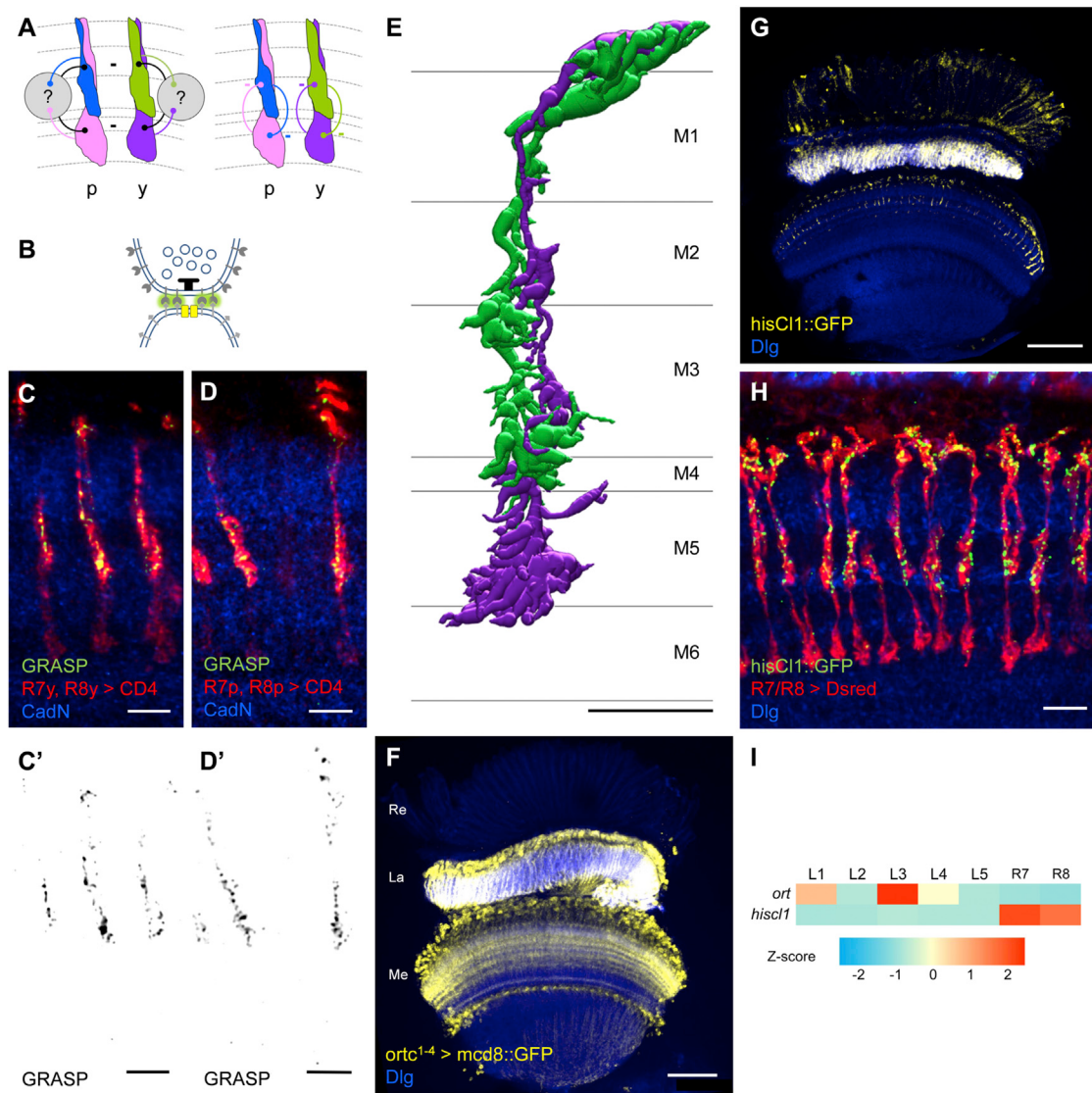


**Figure 5. Genetic and Neuroanatomical Analyses Suggest that R7 and R8 Interact via Direct Synaptic Contacts and the Inhibitory Histamine Receptor HisCl1**

(A) Hypothetical circuits underlying color opponency in p and y R7/R8 terminals. Left: still unidentified interneurons (gray) with a function analogous to horizontal cells in the vertebrate retina receive R7/R8 photoreceptor input and feedback to R7/R8 cells of the same type of ommatidia. Right: R7 and R8 terminals reciprocally inhibit each other directly via chemical synapses.

(B) GRASP enables the identification of synaptic contacts between neurons (Gordon and Scott, 2009).

(C–D') Reconstituted GFP-visualized synaptic contacts between R7 and R8 photoreceptor terminals of y (C) and p (D) ommatidia. Immunolabeling of reconstituted GFP (anti-GFP, green), R7 and R8 cells (anti-CD4, red), and neuropil (anti-cadherin-N [CadN], blue). (C') and (D') show the isolated GRASP signal included in (C) and (D), respectively. Scale bars, 5 μm.

(E) Serial EM reconstruction of R7 and R8 terminals in the medulla (generated based on data from Takemura et al., 2013). Horizontal lines demarcate the medulla layers (M1–M6). Synapse annotation revealed 5 synapses from R7 onto R8 and 11 synapses from R8 onto R7 (Takemura et al., 2013). Scale bar, 5 μm.

(F) *Ort*<sup>c1-4</sup>-GAL4 expressed mcd8::GFP in diverse lamina and medulla neuron types postsynaptic to inner or outer photoreceptors (Gao et al., 2008). GFP is shown in yellow (anti-GFP) and neuropil in blue (anti-Dlg). Scale bar, 50 μm.

(G) A GFP-tagged *hisCl1* gene (Sarov et al., 2016) revealed strong HisCl1 expression (anti-GFP, yellow) in lamina glia cells and additional expression in R7/R8 photoreceptors, including their presynaptic terminals in the medulla neuropil (anti-Dlg, blue). Scale bar, 50 μm.

(H) HisCl1::GFP localized to discrete puncta in the terminals of R7 and R8 photoreceptors in, exclusively, medulla layers M1–M3. Flies and immunolabeling are as in (G), with additional labeling of DsRed in R7/R8 terminals (anti-DsRed, red). Scale bar, 50 μm.

(I) Heatmap showing expression of the *ort* and *hisCl1* genes in lamina monopolar cells (L1–L5) and R7 and R8 cells in pupae. Absolute reads per kilobase of a specific mRNA per million reads (RPKM) are (cell type, *ort*, *hisCl1*) as follows: L1, 8.8, 1.4; L2, 1.6, 1.9; L3, 17.9, 8.5.; L4, 5.0, 4.9; L5, 1.4, 4.3; R7, 0.7, 165.7; and R8, 0.2, 139.8. Based on data from Tan et al. (2015).

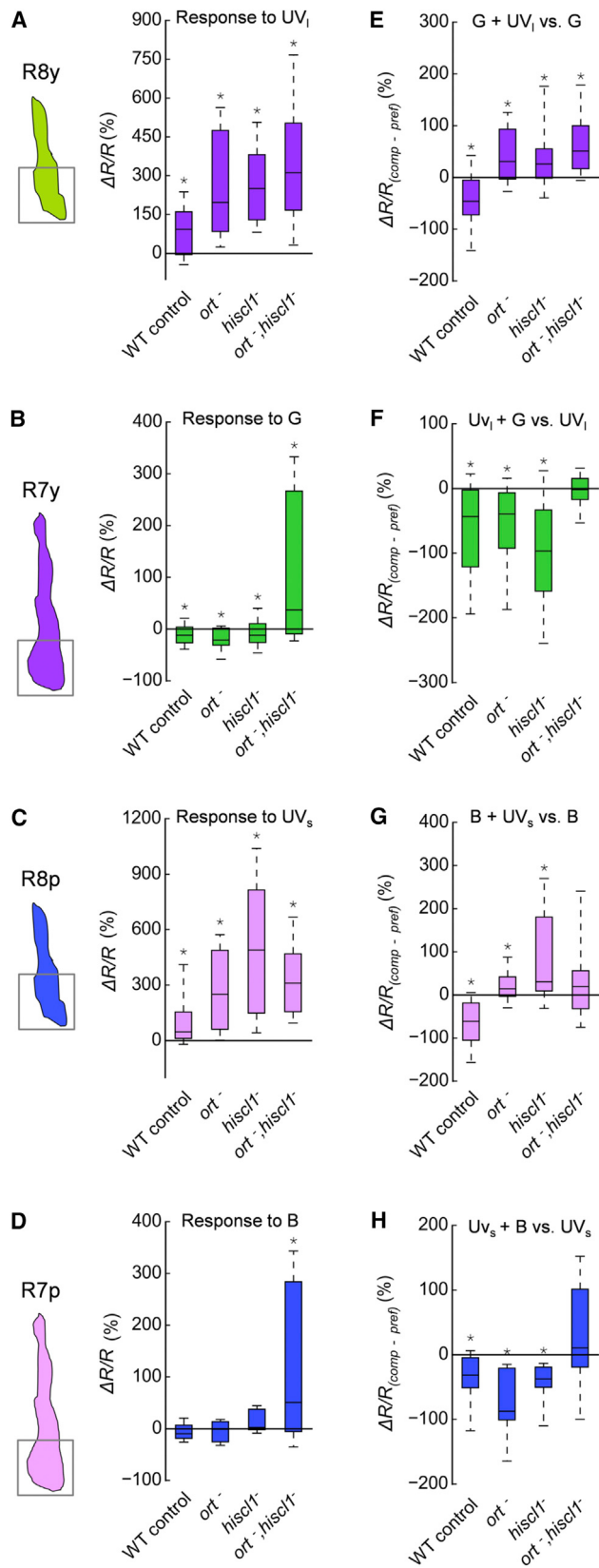


**Figure 6. Ort and HisCl1 Are Differentially Required for Opponent Processing in R7 and R8 Terminals**

(A–D) Maximum responses to opponent monochromatic stimuli in the terminals of (A) R8y (UV<sub>long</sub>), (B) R7y (green), (C) R8p (UV<sub>short</sub>), and (D) R7p (blue) photoreceptors in control, ort<sup>-</sup>, hiscl1<sup>-</sup>, and ort<sup>-</sup>, hiscl1<sup>-</sup> mutant flies (intensity, 10<sup>3</sup> a.u.).

(A and C) R8 terminals of mutants for either or both histamine receptors showed larger responses than R8 terminals of control flies ( $p < 0.05$ , Kruskal-Wallis H test;  $p < 0.05$ , post hoc Mann-Whitney U tests).

(B and D) In R7 terminals, only lack of both histamine receptors caused responses larger than in control flies ( $p < 0.05$ , Kruskal-Wallis H test;  $p < 0.05$ , post hoc Mann-Whitney U tests).

(E–H) Comparison of responses to preferred monochromatic and composite stimuli that include the most efficient inhibitory wavelength (the same genotypes as in A–D). Composite stimuli were as follows: (E) R8y (green + UV<sub>long</sub>), (F) R7y (UV<sub>long</sub> + green), (G) R8p (blue + UV<sub>short</sub>), and (H) R7p (UV<sub>short</sub> + blue). (E and G) R8 terminals in flies mutant for either or both histamine receptors lacked spectral inhibition ( $\Delta R/R_{(comp - pref)}$  not smaller than zero), and  $\Delta R/R_{(comp - pref)}$  was increased compared with control flies ( $p < 0.05$ , Kruskal-Wallis H test;  $p < 0.05$ , post hoc Mann-Whitney U tests).

(F and H) R7 terminals lacked spectral inhibition ( $p > 0.05$ , Wilcoxon test) and exhibited increased  $\Delta R/R_{(comp - pref)}$  compared with control flies ( $p < 0.05$ , Kruskal-Wallis H test;  $p < 0.05$ , post hoc Mann-Whitney U tests) only in mutants for both histamine receptors.

Shown are the same types of plots as in Figures 2 and 3; for n recordings, see Table S1. Asterisks indicate significant difference from R<sub>0</sub> (A–D) and significant inhibition or additional excitation (E–H) ( $p < 0.05$ , Wilcoxon test). See also Figures S6 and S7.

same as in Figure 6) failed to elicit spectral inhibition in all R7 and R8 terminals in negative control flies, and this deficit was restored in all terminals in hisCl1 rescue flies (Figures 7E–7H and S8E–S8H). Taken together, the hisCl1 rescue experiments demonstrate that HisCl1 receptors mediate color-opponent processing in the terminals of inner photoreceptors R7/R8.

## DISCUSSION

Based on the spectral sensitivities of the Rhodopsins expressed in the four types of inner photoreceptors in *Drosophila*, R7 and R8 cells have been implicated in color vision for decades (Heisenberg and Buchner, 1977). Recent studies corroborated this view and provided further insights into the neural underpinnings of *Drosophila* color vision (Gao et al., 2008; Yamaguchi et al., 2010; Schnaitmann et al., 2013; Karuppudurai et al., 2014; Melnattur et al., 2014; Jagadish et al., 2014). However, because of the lack of physiological recordings from neurons in the color pathway, it is still unknown how color information is processed in *Drosophila* at the cellular and circuit level (Behnia and Desplan, 2015). Here we report an optophysiological approach that enables the analysis of neural responses to spectral stimuli in *Drosophila* (Figure 1). Based on this approach, we investigated spectral processing in R7/R8 inner photoreceptor terminals in the medulla. Our study demonstrates that color opponency, a hallmark of spectral processing (Gegenfurtner and Kiper, 2003; Dacey and Packer, 2003; Demb and Singer, 2015), is observable at the level of the first visual synapse in presynaptic terminals of the inner photoreceptors R7/R8 (Figures 2 and 3). Two concurrent neuronal circuit mechanisms that involve distinct histamine receptors (Figure 7I) implement the comparison of R7 and R8 photoreceptor signals in the p and y pathways (Figures 4–7).

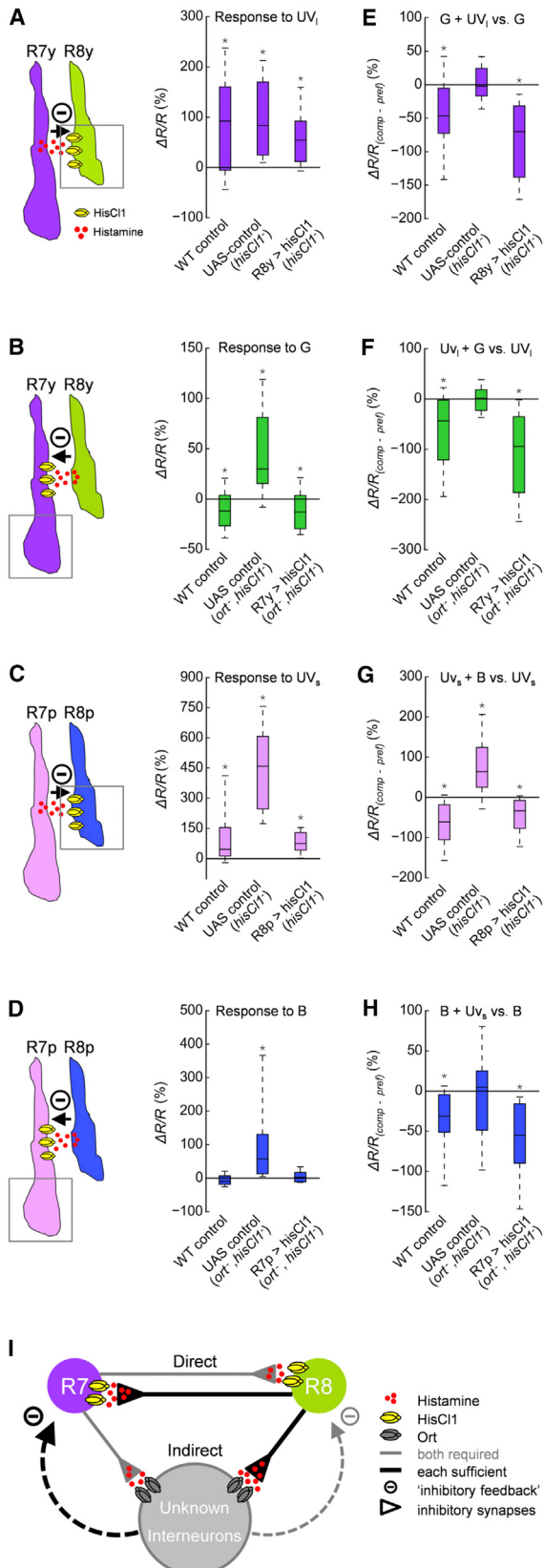


**Figure 7. HisCl1 Rescue in Single Photoreceptor Types Restores Spectral Processing**

(A–D) Maximum responses of photoreceptor terminals to opponent monochromatic stimuli (intensity,  $10^3$  a.u.) in three different genotypes: *hisCl1* rescue flies (*hisCl1*<sup>-</sup> or *hisCl1*<sup>-</sup>/*ort*<sup>-</sup> mutants harboring *UAS-hisCl1* and GAL4-driver), positive control flies (unperturbed circuits), and negative control flies (*hisCl1*<sup>-</sup> or *hisCl1*<sup>-</sup>/*ort*<sup>-</sup> mutants harboring *UAS-hisCl1*). For the exact genotypes, see Table S1. *HisCl1* was rescued in R8y/p and R7y/p cells in *hisCl1*<sup>-</sup> mutant and *hisCl1*<sup>-</sup>/*ort*<sup>-</sup> double mutant flies, respectively (Figure 6). Opponent stimuli were as in Figures 6A–6D.

(A) R8y terminals exhibited comparable responses to monochromatic  $\text{UV}_{\text{long}}$  stimuli in all genotypes ( $p > 0.05$ , Kruskal-Wallis H test).

(B–D) Responses of (B) R7y, (C) R8p, and (D) R7p terminals in *hisCl1* rescue flies were reduced compared with responses in negative control flies ( $p < 0.05$ , Kruskal-Wallis H test;  $p < 0.05$ , post hoc Mann-Whitney U tests) and not different from responses in positive control flies ( $p < 0.05$ , Kruskal-Wallis H test;  $p > 0.05$ , post hoc Mann-Whitney U tests).

(E–H) Comparison of (E) R8y, (F) R7y, (G) R8p, and (H) R7p presynaptic responses to preferred monochromatic stimuli and composite stimuli that included the most efficient opponent wavelength. Same genotypes as in (A)–(D) were used, and visual stimuli were as in Figures 6E–6H. The terminals of all R7/R8 photoreceptor types in *hisCl1* rescue flies showed significant spectral inhibition, similar to the terminals in positive control flies ( $p < 0.05$ , Wilcoxon tests). Spectral inhibition in the terminals of negative control flies was absent ( $\Delta R/R_{(\text{comp} - \text{pref})}$  not smaller than zero).  $\Delta R/R_{(\text{comp} - \text{pref})}$  in R7/R8 terminals in *hisCl1* rescue flies as well as in positive control flies was smaller than in negative control flies ( $p < 0.05$ , Kruskal-Wallis H test;  $p < 0.05$ , post hoc Mann-Whitney U tests).

(A–H) Shown are the same types of plots as in Figures 2 and 3; for n recordings, see Table S1. Asterisks indicate significant difference from  $R_0$  (A–D) and significant inhibition or additional excitation (E–H) ( $p < 0.05$ , Wilcoxon test).

(I) Circuit model of color-opponent processing in R7/R8 terminals. Reciprocal histaminergic synapses between R7 and R8 terminals of the same ommatidium involve HisCl1 receptors and mediate direct inhibitory interactions. An additional unidentified circuit involving neurons that express Ort provides spectral feedback inhibition with the same spectral tuning (p or y) as direct photoreceptor interactions. See also Figure S8.

### Pale and Yellow Color-Opponent Pathways in *Drosophila*

Recordings in *norpA* mutant flies combined with *norpA* rescue in pairwise combinations of photoreceptor types revealed mutual inhibitory interactions between R7 and R8 of the same type of ommatidia (Figures 4 and S2–S5). These interactions provide the cellular basis for  $\text{UV}_{\text{short}}/\text{blue}$  and  $\text{UV}_{\text{long}}/\text{green}$  color-opponent responses in p and y photoreceptor terminals, respectively (see the model in Figure 7I). Similar opponencies were previously posited to underlie color discrimination in dipteran flies (Troje, 1993; Schnaitmann et al., 2013). Thus, we propose that the photoreceptor terminals of the four types of inner photoreceptors mark the onset of two parallel color-opponent pathways that mediate color vision in *Drosophila*.

The recently identified Tm5a/b/c, Tm9, Tm20, and TmY cells that are postsynaptic to R7/R8 (Figures 1B) likely represent further elements of these pathways (Gao et al., 2008; Karuppudurai et al., 2014; Melnattur et al., 2014; Jagadish et al., 2014). In particular, it has been suggested that Tm5a/b/c and Tm20 cells are elements of redundant color vision pathways. Blocking of all of these cell types, but not of single types or combinations, is required for complete loss of color discrimination (Melnattur et al., 2014). Our finding of presynaptic color opponency in R7/R8 photoreceptors suggests that all of these neurons receive

color-opponent input and do not generate color opponency *de novo*. These neurons likely participate in higher color processing, such as the spatial integration of spectral inputs, which is suggested for Tm5b/c cells based on their multi-columnar arborizations. Furthermore, synaptic connections from the outer photoreceptors R1–R6 to L3 lamina neurons and from L3 to some of the candidate neurons (Gao et al., 2008; Takemura et al., 2013) might explain the contribution of R1–R6 to color vision (Schnaitmann et al., 2013). At the level of R7/R8 terminals, we found no evidence for a role of R1–R6 photoreceptors in color-opponent processing (Figures 4 and S2–S5).

### Circuit Mechanisms Underlying Color-Opponent Processing

Our genetic, anatomical, and physiological experiments identify the two *Drosophila* histamine receptors HisCl1 and Ort (Witte et al., 2002; Gao et al., 2008; Pantazis et al., 2008) as key elements of direct and indirect inhibitory circuit mechanisms, respectively (Figure 7I). In prior studies, chemical synaptic contacts of unknown function have been observed between R7/R8 photoreceptors by serial EM (Takemura et al., 2013). Our results on HisCl1 expression (Figures 5G–5H; Tan et al., 2015), GRASP (Figures 5C–5D'), and physiological recording suggest that these synapses are inhibitory and mediate color-opponent processing (Figures 6, 7, and S7). Therefore, HisCl1 is of varying importance in R7 and R8 photoreceptors: in R7 terminals, *hisCl1* expression is not required (Figure 6) but is sufficient to generate color opponency (Figure 7); in R8 terminals, *hisCl1* expression is required for color opponency (Figures 6 and S7), and it is only sufficient when *ort* expression in the visual circuits is intact (Figure 7). Interestingly, the varying importance of *hisCl1*-mediated direct inhibition between R7/R8 correlates well with the reported number of synapses between R7 and R8 photoreceptors. Serial EM reconstruction of one medulla column revealed 5 and 11 synapses from R7 onto R8 and vice versa, respectively (Takemura et al., 2013).

Although *ort* is not expressed in photoreceptors, it nevertheless mediates color-opponent processing in concert with *hisCl1*. Our physiological recordings reveal that *ort* is of varying importance for color opponency in R7 and R8, comparable with the results for *hisCl1*. Intact *ort* expression in the visual circuits is not required but sufficient for color-opponent processing in R7 terminals (Figure 6). In contrast, *ort* expression in the visual circuits is required for color opponency in R8 terminals (Figures 6), and it is only sufficient together with *hisCl1* expression in R8 photoreceptors (Figure 7). The medulla neurons mediating *ort*-dependent feedback inhibition to R7/R8 terminals remain unknown. Among the many *ort*-expressing neurons in the medulla (Figure 5F), several neuron types have been identified (Gao et al., 2008; Pantazis et al., 2008); however, none of these cell types establish feedback synapses onto R7/R8 photoreceptors (Gao et al., 2008; Takemura et al., 2013; Karuppudurai et al., 2014).

Work on polarization vision in flies has demonstrated that inner photoreceptors in the dorsal rim area similarly display antagonistic responses when the orientation of the e-vector is altered (Weir et al., 2016; Hardie, 1984). If these inhibitory interactions are mediated by circuit mechanisms similar to the ones

described in our study remains to be investigated. Along with our results, the prior findings of Weir et al. (2016) suggest that presynaptic calcium in *Drosophila* photoreceptor terminals is altered by local circuit interactions that enhance contrast.

Because the distal segments of the inner photoreceptors of large flies and of most other insects exhibit exclusively depolarizing non-opponent voltage responses (Hardie, 1977; Smola and Meffert, 1979; Introduction), the observed color opponency in *Drosophila* inner photoreceptor terminals is unexpected, and we propose that spectrally antagonistic processing emerges only locally in photoreceptor terminals. Assuming that this local inhibitory signal does not propagate backward to the distal photoreceptor segments that have been recorded intracellularly, local processing would explain and reconcile the reported differences between insect species.

### *Drosophila* and Vertebrates Implement Color-Opponent Processing at the First Visual Synapse in Different Ways

Our recordings from R7/R8 terminals are consistent with mutually antagonistic processing of photoreceptors in the vertebrate retina (Gegenfurtner and Kiper, 2003; Dacey and Packer, 2003; Demb and Singer, 2015). However, substantial differences in the molecular, synaptic, and network implementation demonstrate surprising variability in the underlying circuits.

Vertebrate photoreceptors employ cyclic guanosine monophosphate (cGMP) signaling, hyperpolarize, and reduce the release of glutamate in response to light. As a consequence, horizontal cells and OFF-bipolar cells expressing sign-conserving  $\alpha$ -amino-3-hydroxy-5-methyl-4-isoxazol-propionic acid (AMPA)/kainate-receptors receive less excitation, whereas ON-bipolar cells expressing sign-inverting metabotropic glutamate receptor 6 (mGluR6) receive less inhibition (Wässle, 2004; Demb and Singer, 2015). In contrast, *Drosophila* photoreceptors employ phosphoinositide signaling and depolarize in response to light (Hardie and Juusola, 2015). This increases presynaptic calcium influx and the release of histamine, which binds to inhibitory Ort and HisCl1 receptors on postsynaptic cells.

Our results show that, in addition to interactions with Ort-expressing second-order neurons of the medulla, direct HisCl1-mediated interactions between inner photoreceptors play an important role in *Drosophila* color vision (Figures 5–7, S7 and S8). Direct chemical synaptic interactions between different types of cones do not exist in the vertebrate retina (Wässle, 2004; Demb and Singer, 2015). Vertebrate horizontal cells are the key players in early color-opponent processing: they receive input from different types of cones, synapse onto bipolar cells, and feed back onto cones with a sign-inverting synapse. Light-induced disinhibition of cone terminals is the fundamental mechanism underlying opponent L/M, and S/(L+M) interactions in cone terminals (Dacey and Packer, 2003; Wässle, 2004; Chapot et al., 2017). If neurons analogous to horizontal cells exist in the *Drosophila* visual system has to be revealed. If so, they should participate in the Ort-dependent opponency mechanism revealed here (Figure 7I). Based on our data and similar findings regarding the vertebrate retina, we propose that presynaptic color opponency in photoreceptor terminals is an important processing principle of color vision that is shared across taxa and that evolved in different taxa independently.

## STAR★METHODS

Detailed methods are provided in the online version of this paper and include the following:

- KEY RESOURCES TABLE
- CONTACT FOR REAGENT AND RESOURCE SHARING
- EXPERIMENTAL MODEL AND SUBJECT DETAILS
  - Flies
- METHOD DETAILS
  - Two-photon calcium imaging
  - Visual stimulus presentation
  - Molecular biology and generation of transgenic flies
  - Verification of targeted hisCl1 expression
  - Immunohistochemistry
  - 3D rendering of R7/R8 photoreceptor EM-reconstructions
- QUANTIFICATION AND STATISTICAL ANALYSIS
  - Calcium imaging
  - Statistics
- DATA AND SOFTWARE AVAILABILITY

## SUPPLEMENTAL INFORMATION

Supplemental Information includes eight figures and one table and can be found with this article online at <https://doi.org/10.1016/j.cell.2017.12.018>.

## ACKNOWLEDGMENTS

We thank B. Ziser, K. Eschbach, L. Gladis, and A. Laurencio for excellent technical assistance; the mechanics workshop of the Institute of Biology I, especially H. Noeske; and the Life Imaging Center Freiburg (LIC), especially R. Nitschke. We thank C. Desplan, R. Hardie, and H. Bellen for fly stocks and C.-H. Lee for fly stocks and DNA. We are grateful to R. Menzel, M. Heisenberg, R. Friedrich, and A. Straw for comments on an early version and to M. Dickinson for his thorough comments on the final manuscript. This work was supported by a grant for major instrumentation (91b GG to D.F.R.) funded by the German Research Foundation (DFG - INST 39/902-1) and the state of Baden-Württemberg.

## AUTHOR CONTRIBUTIONS

D.F.R and V.H. built the 2PLSM microscope. C.S. and V.H. designed the LED-based visual stimulation device. C.S. and D.F.R. designed and interpreted all experiments. C.S. performed and analyzed all physiological recordings in photoreceptors. E.A., V.O., and D.F.R. generated transgenic flies and tested calcium indicators in flies. V.O. designed the genomic analysis of *rh6<sup>7</sup>*. T.T. and O.G. provided Twitch-2C DNA. C.S. and D.F.R. wrote the manuscript. O.G., V.O., and V.H. revised the manuscript.

## DECLARATION OF INTERESTS

The authors declare no competing interests.

Received: January 27, 2017

Revised: October 3, 2017

Accepted: December 14, 2017

Published: January 11, 2018

## REFERENCES

- Abramov, I., and Gordon, J. (1994). Color appearance: on seeing red—or yellow, or green, or blue. *Annu. Rev. Psychol.* **45**, 451–485.
- Arikawa, K., Wakakuwa, M., Qiu, X., Kurasawa, M., and Stavenga, D.G. (2005). Sexual dimorphism of short-wavelength photoreceptors in the small white butterfly, *Pieris rapae crucivora*. *J. Neurosci.* **25**, 5935–5942.
- Ascoli, G.A., Donohue, D.E., and Halavi, M. (2007). NeuroMorpho.Org: a central resource for neuronal morphologies. *J. Neurosci.* **27**, 9247–9251.
- Behnia, R., and Desplan, C. (2015). Visual circuits in flies: beginning to see the whole picture. *Curr. Opin. Neurobiol.* **34**, 125–132.
- Chapot, C.A., Euler, T., and Schubert, T. (2017). How do horizontal cells ‘talk’ to cone photoreceptors? Different levels of complexity at the cone-horizontal cell synapse. *J. Physiol.* **595**, 5495–5506.
- Chen, P.J., Arikawa, K., and Yang, E.C. (2013). Diversity of the photoreceptors and spectral opponency in the compound eye of the Golden Birdwing, *Troides aeacus formosanus*. *PLoS ONE* **8**, e62240.
- Clarke, S.E., Longtin, A., and Maler, L. (2015). Contrast coding in the electro-sensory system: parallels with visual computation. *Nat. Rev. Neurosci.* **16**, 733–744.
- Dacey, D.M., and Packer, O.S. (2003). Colour coding in the primate retina: diverse cell types and cone-specific circuitry. *Curr. Opin. Neurobiol.* **13**, 421–427.
- Demb, J.B., and Singer, J.H. (2015). Functional circuitry of the retina. *Annu. Rev. Vis. Sci.* **1**, 263–289.
- Gao, S., Takemura, S.Y., Ting, C.Y., Huang, S., Lu, Z., Luan, H., Rister, J., Thum, A.S., Yang, M., Hong, S.-T., et al. (2008). The neural substrate of spectral preference in *Drosophila*. *Neuron* **60**, 328–342.
- Gegenfurtner, K.R., and Kiper, D.C. (2003). Color vision. *Annu. Rev. Neurosci.* **26**, 181–206.
- Gordon, M.D., and Scott, K. (2009). Motor control in a *Drosophila* taste circuit. *Neuron* **61**, 373–384.
- Hardie, R.C. (1977). Electrophysiological properties of R7 and R8 in dipteran retina. *Z. Naturforsch. C* **32c**, 887–889.
- Hardie, R.C. (1984). Properties of photoreceptors R7 and R8 in dorsal marginal ommatidia in the compound eyes of *Musca* and *Calliphora*. *J. Comp. Physiol. A Neuroethol. Sens. Neural Behav. Physiol.* **154**, 157–165.
- Hardie, R.C. (1989). A histamine-activated chloride channel involved in neurotransmission at a photoreceptor synapse. *Nature* **339**, 704–706.
- Hardie, R.C., and Juusola, M. (2015). Phototransduction in *Drosophila*. *Curr. Opin. Neurobiol.* **34**, 37–45.
- Heisenberg, M., and Buchner, E. (1977). The role of retinula cell types in visual behavior of *Drosophila melanogaster*. *J. Comp. Physiol.* **117**, 127–162.
- Horridge, G.A., Marcelja, L., Jahnke, R., and Matic, T. (1983). Single electrode studies on the retina of the butterfly *Papilio*. *J. Comp. Physiol.* **150**, 271–294.
- Inoue, H., Yoshioka, T., and Hotta, Y. (1985). A genetic study of inositol triphosphate involvement in phototransduction using *Drosophila* mutants. *Biochem. Biophys. Res. Commun.* **132**, 513–519.
- Jagadish, S., Barnea, G., Clandinin, T.R., and Axel, R. (2014). Identifying functional connections of the inner photoreceptors in *Drosophila* using Tango-Trace. *Neuron* **83**, 630–644.
- Jones, P.L., and Agrawal, A.A. (2017). Learning in insect pollinators and herbivores. *Annu. Rev. Entomol.* **62**, 53–71.
- Karuppudurai, T., Lin, T.Y., Ting, C.Y., Pursley, R., Melnattur, K.V., Diao, F., White, B.H., Macpherson, L.J., Gallio, M., Pohida, T., and Lee, C.H. (2014). A hard-wired glutamatergic circuit pools and relays UV signals to mediate spectral preference in *Drosophila*. *Neuron* **81**, 603–615.
- Kelber, A. (2016). Colour in the eye of the beholder: receptor sensitivities and neural circuits underlying colour opponency and colour perception. *Curr. Opin. Neurobiol.* **41**, 106–112.
- Kelber, A., Vorobyev, M., and Osorio, D. (2003). Animal colour vision—behavioural tests and physiological concepts. *Biol. Rev. Camb. Philos. Soc.* **78**, 81–118.
- Kien, J., and Menzel, R. (1977). Chromatic properties of interneurons in the optic lobes of the bee; II. Narrow band and colour opponent neurons. *J. Comp. Physiol.* **113**, 35–53.

- Mank, M., Reiff, D.F., Heim, N., Friedrich, M.W., Borst, A., and Griesbeck, O. (2006). A FRET-based calcium biosensor with fast signal kinetics and high fluorescence change. *Biophys. J.* **90**, 1790–1796.
- Markstein, M., Pitsouli, C., Villalta, C., Celtniker, S.E., and Perrimon, N. (2008). Exploiting position effects and the gypsy retrovirus insulator to engineer precisely expressed transgenes. *Nat. Genet.* **40**, 476–483.
- Matic, T. (1983). Electrical inhibition in the retina of the butterfly *Papilio*. I. Four spectral types of photoreceptors. *J. Comp. Physiol.* **152**, 169–182.
- Melnattur, K.V., Pursley, R., Lin, T.Y., Ting, C.Y., Smith, P.D., Pohida, T., and Lee, C.H. (2014). Multiple redundant medulla projection neurons mediate color vision in *Drosophila*. *J. Neurogenet.* **28**, 374–388.
- Menzel, R., Ventura, D.F., Hertel, H., de Souza, J., and Greggers, U. (1986). Spectral sensitivity of photoreceptors in insect compound eyes: comparison of species and methods. *J. Comp. Physiol. A Neuroethol. Sens. Neural Behav. Physiol.* **158**, 165–177.
- Oh, Y., Jang, D., Sonn, J.Y., and Choe, J. (2013). Histamine-HisCl<sub>1</sub> receptor axis regulates wake-promoting signals in *Drosophila melanogaster*. *PLoS ONE* **8**, e68269.
- Olsen, S.R., and Wilson, R.I. (2008). Lateral presynaptic inhibition mediates gain control in an olfactory circuit. *Nature* **452**, 956–960.
- Pantazis, A., Segaran, A., Liu, C.H., Nikolaev, A., Rister, J., Thum, A.S., Roeder, T., Semenov, E., Juusola, M., and Hardie, R.C. (2008). Distinct roles for two histamine receptors (hclA and hclB) at the *Drosophila* photoreceptor synapse. *J. Neurosci.* **28**, 7250–7259.
- Paulk, A.C., Dacks, A.M., and Gronenberg, W. (2009). Color processing in the medulla of the bumblebee (Apidae: *Bombus impatiens*). *J. Comp. Neurol.* **513**, 441–456.
- Peitsch, D., Fietz, A., Hertel, H., de Souza, J., Ventura, D.F., and Menzel, R. (1992). The spectral input systems of hymenopteran insects and their receptor-based colour vision. *J. Comp. Physiol. A Neuroethol. Sens. Neural Behav. Physiol.* **170**, 23–40.
- Pfeiffer, B.D., Ngo, T.T., Hibbard, K.L., Murphy, C., Jenett, A., Truman, J.W., and Rubin, G.M. (2010). Refinement of tools for targeted gene expression in *Drosophila*. *Genetics* **186**, 735–755.
- Qiu, X., and Arikawa, K. (2003). The photoreceptor localization confirms the spectral heterogeneity of ommatidia in the male small white butterfly, *Pieris rapae crucivora*. *J. Comp. Physiol. A Neuroethol. Sens. Neural Behav. Physiol.* **189**, 81–88.
- Reiff, D.F., Plett, J., Mank, M., Griesbeck, O., and Borst, A. (2010). Visualizing retinotopic half-wave rectified input to the motion detection circuitry of *Drosophila*. *Nat. Neurosci.* **13**, 973–978.
- Rushton, W.A.H. (1972). Pigments and signals in colour vision. *J. Physiol.* **220**, 1P.
- Salcedo, E., Huber, A., Henrich, S., Chadwell, L.V., Chou, W.H., Paulsen, R., and Britt, S.G. (1999). Blue- and green-absorbing visual pigments of *Drosophila*: ectopic expression and physiological characterization of the R8 photoreceptor cell-specific Rh5 and Rh6 rhodopsins. *J. Neurosci.* **19**, 10716–10726.
- Sarov, M., Barz, C., Jambor, H., Hein, M.Y., Schmied, C., Suchold, D., Stender, B., Janosch, S., K.J., V.V., Krishnan, R.T., et al. (2016). A genome-wide resource for the analysis of protein localisation in *Drosophila*. *eLife* **5**, e12068.
- Schmeling, F., Wakakuwa, M., Tegtmeier, J., Kinoshita, M., Bockhorst, T., Ariyama, K., and Homberg, U. (2014). Opsin expression, physiological characterization and identification of photoreceptor cells in the dorsal rim area and main retina of the desert locust, *Schistocerca gregaria*. *J. Exp. Biol.* **217**, 3557–3568.
- Schnaitmann, C., Garbers, C., Wachtler, T., and Tanimoto, H. (2013). Color discrimination with broadband photoreceptors. *Curr. Biol.* **23**, 2375–2382.
- Skorupski, P., and Chittka, L. (2010). Photoreceptor spectral sensitivity in the bumblebee, *Bombus impatiens* (Hymenoptera: Apidae). *PLoS ONE* **5**, e12049.
- Smola, U., and Meffert, P. (1979). The spectral sensitivity of the visual cells R7 and R8 in the eye of the blowfly *Calliphora erythrocephala*. *J. Comp. Physiol.* **133**, 41–52.
- Takemura, S.Y., Karuppudurai, T., Ting, C.Y., Lu, Z., Lee, C.H., and Meinertz-hagen, I.A. (2011). Cholinergic circuits integrate neighboring visual signals in a *Drosophila* motion detection pathway. *Curr. Biol.* **21**, 2077–2084.
- Takemura, S.Y., Bharioke, A., Lu, Z., Nern, A., Vitaladevuni, S., Rivlin, P.K., Katz, W.T., Olbris, D.J., Plaza, S.M., Winston, P., et al. (2013). A visual motion detection circuit suggested by *Drosophila* connectomics. *Nature* **500**, 175–181.
- Tan, L., Zhang, K.X., Pecot, M.Y., Nagarkar-Jaiswal, S., Lee, P.T., Takemura, S.Y., McEwen, J.M., Nern, A., Xu, S., Tadros, W., et al. (2015). Ig superfamily ligand and receptor pairs expressed in synaptic partners in *Drosophila*. *Cell* **163**, 1756–1769.
- Thestrup, T., Litzlbauer, J., Bartholomäus, I., Mues, M., Russo, L., Dana, H., Kovalchuk, Y., Liang, Y., Kalamakis, G., Laukat, Y., et al. (2014). Optimized ratiometric calcium sensors for functional in vivo imaging of neurons and T lymphocytes. *Nat. Methods* **11**, 175–182.
- Troje, N. (1993). Spectral categories in the learning behaviour of blowflies. *Z. Naturforsch.* **48c**, 96–104.
- Venken, K.J., He, Y., Hoskins, R.A., and Bellen, H.J. (2006). P[acman]: a BAC transgenic platform for targeted insertion of large DNA fragments in *D. melanogaster*. *Sci* **314**, 1747–1751.
- Wardill, T.J., List, O., Li, X., Dongre, S., McCulloch, M., Ting, C.Y., O'Kane, C.J., Tang, S., Lee, C.H., Hardie, R.C., and Juusola, M. (2012). Multiple spectral inputs improve motion discrimination in the *Drosophila* visual system. *Sci* **336**, 925–931.
- Wässle, H. (2004). Parallel processing in the mammalian retina. *Nat. Rev. Neurosci.* **5**, 747–757.
- Weir, P.T., Henze, M.J., Bleul, C., Baumann-Klausener, F., Labhart, T., and Dickinson, M.H. (2016). Anatomical reconstruction and functional imaging reveal an ordered array of skylight polarization detectors in *Drosophila*. *J. Neurosci.* **36**, 5397–5404.
- Wernet, M.F., Mazzoni, E.O., Çelik, A., Duncan, D.M., Duncan, I., and Desplan, C. (2006). Stochastic spineless expression creates the retinal mosaic for colour vision. *Nature* **440**, 174–180.
- Witte, I., Kreienkamp, H.J., Gewecke, M., and Roeder, T. (2002). Putative histamine-gated chloride channel subunits of the insect visual system and thoracic ganglion. *J. Neurochem.* **83**, 504–514.
- Yamaguchi, S., Wolf, R., Desplan, C., and Heisenberg, M. (2008). Motion vision is independent of color in *Drosophila*. *Proc. Natl. Acad. Sci. USA* **105**, 4910–4915.
- Yamaguchi, S., Desplan, C., and Heisenberg, M. (2010). Contribution of photoreceptor subtypes to spectral wavelength preference in *Drosophila*. *Proc. Natl. Acad. Sci. USA* **107**, 5634–5639.

## STAR★METHODS

## KEY RESOURCES TABLE

REAGENT or RESOURCE	SOURCE	IDENTIFIER
<b>Antibodies</b>		
rabbit anti-GFP	Abcam	#ab290; RRID:AB_303395
mouse anti-GFP	Sigma	#G6539; RRID:AB_259941
rabbit anti-CD4	Sigma	#HPA004252; RRID:AB_1078466
rat anti-CadN	DSHB	#DN-Ex #8; RRID:AB_2619582
mouse anti-Dlg	DSHB	#4F3; RRID:AB_528203
goat anti-rabbit Alexa Fluor 488	Life Technologies	#A-11008; RRID:AB_143165
goat anti-mouse Alexa Fluor 488	Life Technologies	#A-11001; RRID:AB_2534069
goat anti-rabbit Alexa Fluor 555	Life Technologies	#A-21430; RRID:AB_2535851
goat anti-rat Alexa Fluor 405	Abcam	#ab175671
goat anti-mouse Alexa Fluor 633	Life Technologies	#A-21053; RRID:AB_1500753
<b>Chemicals, Peptides, and Recombinant Proteins</b>		
TRIzol® Reagent	Ambion by Life Technologies	#15596-018
SuperScript®III First-Strand Synthesis System for RT-PCR	Invitrogen by Life Technologies	#18080-051 MAN0001346
<b>Experimental Models: Organisms/Strains</b>		
<i>Drosophila: rh1-GAL4</i>	Bloomington Stock Center	#8688
<i>Drosophila: rh3-GAL4</i>	Bloomington Stock Center	#7457
<i>Drosophila: rh4-GAL4</i>	Bloomington Stock Center	#8627
<i>Drosophila: rh5-GAL4</i>	Bloomington Stock Center	#7458
<i>Drosophila: rh6-GAL4</i>	Bloomington Stock Center	#7459
<i>Drosophila: rh3-LexA (attp40)</i>	Reiff Lab, University of Freiburg, This paper	N/A
<i>Drosophila: rh3-LexA (VK00027)</i>	Reiff Lab, University of Freiburg, This paper	N/A
<i>Drosophila: rh4-LexA (attp40)</i>	Reiff Lab, University of Freiburg, This paper	N/A
<i>Drosophila: rh4-LexA (VK00027)</i>	Reiff Lab, University of Freiburg, This paper	N/A
<i>Drosophila: rh5-LexA (attp40)</i>	Reiff Lab, University of Freiburg, This paper	N/A
<i>Drosophila: rh6-LexA (attp40)</i>	Reiff Lab, University of Freiburg, This paper	N/A
<i>Drosophila: rh6-LexA (VK00027)</i>	Reiff Lab, University of Freiburg, This paper	N/A
<i>Drosophila: UAS-twitch-2C (attp40)</i>	Reiff Lab, University of Freiburg, This paper	N/A
<i>Drosophila: LexAop-twitch-2C (attp40)</i>	Reiff Lab, University of Freiburg, This paper	N/A
<i>Drosophila: LexAop-twitch-2C (VK00027)</i>	Reiff Lab, University of Freiburg, This paper	N/A
<i>Drosophila: UAS-TNXL</i>	Borst Lab, Max-Planck-Institute of Neurobiology, Mank et al., 2006	N/A
<i>Drosophila: UAS-norpA.K(1)</i>	Bloomington Stock Center	#26267
<i>Drosophila: norpA<sup>7</sup></i>	Bloomington Stock Center	#5685
<i>Drosophila: UAS-CD4-spGFP1-10 (VK00027), lexAop-CD4-spGFP11 (VK00005)</i>	Reiff Lab, University of Freiburg, This paper	N/A
<i>Drosophila: ort<sup>c1-4</sup>-GAL4</i>	Lee Lab, NIH, Gao et al., 2008	N/A
<i>Drosophila: hisCl1-GAL4</i>	Hardie Lab, University of Cambridge, Pantazis et al., 2008	N/A
<i>Drosophila: UAS-mCD8::GFP</i>	Bloomington Stock Center, Pfeiffer et al., 2010	#32186
<i>Drosophila: hisCl1::GFP<sup>TRG.1051</sup></i>	VDRC, Sarov et al., 2016	#318735
<i>Drosophila: Mlp84B::GFP<sup>TRG.678</sup></i>	VDRC, Sarov et al., 2016	#318177

(Continued on next page)

**Continued**

REAGENT or RESOURCE	SOURCE	IDENTIFIER
<i>Drosophila: Unc-89::GFP<sup>TRG.1057</sup></i>	VDRC, <a href="#">Sarov et al., 2016</a>	#318326
<i>Drosophila: ort<sup>1</sup>,ninaE<sup>1</sup></i>	Bloomington Stock Center	#1133
<i>Drosophila: ort<sup>ws2515</sup></i>	Pak Lab, Purdue University	N/A
<i>Drosophila: hisCl1<sup>384</sup></i>	Yangkyun Oh, KAIST, <a href="#">Oh et al., 2013</a>	N/A
<i>Drosophila: ort<sup>P306</sup>,hisCl1<sup>134</sup></i>	Lee Lab, NIH, <a href="#">Gao et al., 2008</a>	N/A
<i>Drosophila: ort<sup>1</sup>,ninaE<sup>1</sup>,rh6<sup>1</sup>,hisCl1<sup>134</sup></i>	Lee Lab, NIH, <a href="#">Gao et al., 2008</a>	N/A
<i>Drosophila: UAS-hisCl1(su(Hw)attP5)</i>	Reiff Lab, University of Freiburg, This paper	N/A
<i>Drosophila: UAS-hisCl1-RNAi</i>	VDRC	#104966
<i>Drosophila: UAS-dcr2</i>	Bloomington Stock Center	#24651
<i>Drosophila: y<sup>1</sup>v<sup>1</sup>P{nos-phiC31\int.NLS}X; P{CarryP}attP40</i>	Bloomington Stock Center	#25709
<i>Drosophila: y<sup>1</sup>w<sup>*</sup>P{nos-phiC31\int.NLS}X; PBac{y<sup>+</sup>-attP-9A}VK00027</i>	Bloomington Stock Center	#35569
<i>Drosophila: y<sup>1</sup>w<sup>*</sup>P{nos-phiC31\int.NLS}X; P{CarylP}su(Hw)attP5</i>	Bloomington Stock Center	#32231
<i>Drosophila: y<sup>1</sup>w<sup>1118</sup>P{nos-phiC31\int.NLS}X; PBac{y[+] -attP}VK00005</i>	Bellen Lab, Baylor College of Medicine, <a href="#">Venken et al., 2006</a>	N/A
<b>Oligonucleotides</b>		
Primer: rh3-Promoter-Forward: 5'-ggg gac cac ttt gta caa gaa agc tgg gtc tgc ggg cca-3'	Reiff Lab, University of Freiburg, This paper	N/A
Primer: rh3-Promoter-Reverse: 5'-ggg gac cac ttt gta caa gaa agc tgg gtc tgc ggg cca aga -3'	Reiff Lab, University of Freiburg, This paper	N/A
Primer: rh4-Promoter-Forward: 5'-ggg gac aag ttt gta caa aaa agc agg cta tcc gct cgt tgc ttg cgt atg -3'	Reiff Lab, University of Freiburg, This paper	N/A
Primer: rh4-Promoter-Reverse: 5'-ggg gac cac ttt gta caa gaa agc tgg gtc ggt caa ccc gat acc gaa ccg -3'	Reiff Lab, University of Freiburg, This paper	N/A
Primer: rh6 Forward: 5'-tcg gct gga atc ggt atg tg-3'	Reiff Lab, University of Freiburg, This paper	N/A
Primer: rh6 Reverse: 5'-tga tct cga tgg cct tgc tc-3'	Reiff Lab, University of Freiburg, This paper	N/A
Primer: hisCl1 Forward: 5'-atc tcg agc aat gag tgc cag agg aac aat atc-3'	Reiff Lab, University of Freiburg, This paper	N/A
Primer: hisCl1 Reverse: 5'-gct cta gac ctt cgg aga aac ttt tcc atc-3'	Reiff Lab, University of Freiburg, This paper	N/A
Primer: hisCl1 (RT-PCR) Forward: 5'-atc tcg agc aat gag tgc cag agg aac aat atc-3'	Reiff Lab, University of Freiburg, This paper	N/A
Primer: hisCl1 (RT-PCR) Reverse: 5'-cta gaa acg ctt tcc ttt att tat aca cta cat gg-3'	Reiff Lab, University of Freiburg, This paper	N/A
Primer: Actin-Forward: 5'-gtt tga gtt ctt gtg ctg tgt gga tac tcc-3'	Reiff Lab, University of Freiburg, This paper	N/A
Primer: Actin-Reverse: 5'-gaa ggt ctc gaa cat gat ctg ggt cat g-3'	Reiff Lab, University of Freiburg, This paper	N/A
<b>Recombinant DNA</b>		
<i>Twitch-2B pRSETB</i>	Griesbeck Lab, Max Planck Institute of Neurobiology, <a href="#">Thestrup et al., 2014</a>	N/A
<i>pUAST</i>	Perrimon Lab, Harvard Medical School, <a href="#">Markstein et al., 2008</a>	N/A
<i>pCa4B2G</i>	Perrimon Lab, Harvard Medical School, <a href="#">Markstein et al., 2008</a>	N/A
<i>pJFRC19-13XLexAop2-IVS-myr::GFP</i>	Addgene, <a href="#">Pfeiffer et al., 2010</a>	#26224
<i>pJFRC2-10xUAS-IVS-mCD8::GFP</i>	Addgene, <a href="#">Pfeiffer et al., 2010</a>	#26214
<i>pCaST-rh3-norpA</i>	Lee Lab, NIH, <a href="#">Wardill et al., 2012</a>	N/A
<i>pCaST-rh4-norpA</i>	Lee Lab, NIH, <a href="#">Wardill et al., 2012</a>	N/A

(Continued on next page)

**Continued**

REAGENT or RESOURCE	SOURCE	IDENTIFIER
<i>pCaST-rh5-norpA</i>	Lee Lab, NIH, Wardill et al., 2012	N/A
<i>pCaST-rh6-norpA</i>	Lee Lab, NIH, Wardill et al., 2012	N/A
Software and Algorithms		
Fiji	NIH	<a href="https://fiji.sc/">https://fiji.sc/</a>
ImageJ (MBF)	NIH	<a href="http://imagej.net/mbf/">http://imagej.net/mbf/</a>
Python 2.7	Python Software Foundation	<a href="https://www.python.org/">https://www.python.org/</a>
SciPy	SciPy	<a href="https://www.scipy.org/">https://www.scipy.org/</a>
SharkViewer	Janelia Research Campus, HHMI	<a href="https://github.com/JaneliaSciComp/SharkViewer">https://github.com/JaneliaSciComp/SharkViewer</a>
Calcium Imaging Analysis Code	Reiff Lab, University of Freiburg, This paper	N/A

**CONTACT FOR REAGENT AND RESOURCE SHARING**

Further information and requests for resources and reagents should be directed to and will be fulfilled by the Lead Contact, Dierk F. Reiff ([dierk.reiff@biologie.uni-freiburg.de](mailto:dierk.reiff@biologie.uni-freiburg.de)).

**EXPERIMENTAL MODEL AND SUBJECT DETAILS****Flies**

Flies were raised on standard cornmeal medium at 60% relative humidity at a 14/10 h light/dark cycle. Flies were reared at 25°C except for the flies used in *hisCl1* rescue experiments that were reared at 18°C. Female flies (*white*<sup>+</sup>) 2 – 6 days after eclosion were used in all experiments. *rh1-GAL4* (1<sup>st</sup>), *rh3-GAL4* (2<sup>nd</sup>), *rh4-GAL4* (2<sup>nd</sup>), *rh5-GAL4* (2<sup>nd</sup>), *rh6-GAL4* (2<sup>nd</sup>) were used to express *UAS-twitch-2C* (2<sup>nd</sup>, attp40, see below), and *rh3-LexA* (2<sup>nd</sup>, attp40; 3<sup>rd</sup>, VK00027, see below), *rh4-LexA* (2<sup>nd</sup>, attp40; 3<sup>rd</sup>, VK00027, see below), *rh5-LexA* (2<sup>nd</sup>, attp40, see below), *rh6-LexA* (2<sup>nd</sup>, attp40; 3<sup>rd</sup>, VK00027, see below) were used to express *LexAop-twitch-2C* (2<sup>nd</sup>, attp40; 3<sup>rd</sup>, VK00027; see below) in R1–R6, R7p, R7y, R8p, and R8y photoreceptors, respectively. The genetic calcium sensor Twitch-2C is described in (Thestrup et al., 2014). To compare the kinetics of the Twitch-2C fluorescence changes we used flies expressing the fast and low affinity calcium reporter *UAS-TNXL* (2<sup>nd</sup>, (Mank et al., 2006)). *Rhodopsin-GAL4* driver lines were kindly provided by Claude Desplan. *UAS-norpA.K(1)* (Bloomington Stock Center, 26267) was used to restore *norpA*-function in *norpA*<sup>7</sup> null mutants (Bloomington Stock Center, 5685). For GRASP analysis, we used a recombinant fly strain combined of *UAS-CD4-spGFP1-10* (3<sup>rd</sup>, VK00027, see below), and *LexAop-CD4-spGFP11* (3<sup>rd</sup>, VK00005, see below) (Gordon and Scott, 2009) together with combinations of the previously mentioned *rhodopsin-GAL4* and -*LexA* driver lines. *ort*<sup>c1-4</sup>-*GAL4* (Gao et al., 2008) and *hisCl1-GAL4* (Pantazis et al., 2008) were used to express *UAS-mCD8::GFP* (Bloomington Stock Center, 32186) (Pfeiffer et al., 2010) in *ort*- and *hisCl1*-positive neurons. To visualize *hisCl1*-positive neurons and to localize HisCl1 protein we used *yw*; *hisCl1::GFP*<sup>fTRG.1051</sup> (VDRC, 318735) and different negative controls *yw*; *Mlp84B::GFP*<sup>fTRG.468</sup> (VDRC, 318177), *yw*; *Unc-89::GFP*<sup>fTRG.1046</sup> (VDRC, 318326) (all flies from (Sarov et al., 2016)). For analysis of histamine receptor requirement we used *ort*<sup>1</sup>,*ninaE*<sup>1</sup> (Bloomington Stock Center, 1133), *ort*<sup>us2515</sup> (kindly provided by William Pak), *hisCl1*<sup>384</sup> (kindly provided by Yangkyun Oh (Oh et al., 2013)), *ort*<sup>P306</sup>,*hisCl1*<sup>134</sup> and *ort*<sup>1</sup>,*ninaE*<sup>1</sup>,*rh6*<sup>1</sup>,*hisCl1*<sup>134</sup> (kindly provided by Chi-Hon Lee (Karuppudurai et al., 2014; Gao et al., 2008)). PCR-analysis revealed that the *ort*,*hisCl1*<sup>−</sup> double mutant (previously named *ort*<sup>1</sup>,*hisCl1*<sup>134</sup> (Gao et al., 2008) or *ort*<sup>1</sup>,*ninaE*<sup>1</sup>,*hisCl1*<sup>134</sup> (Karuppudurai et al., 2014))) in addition carries a *rh6*<sup>1</sup> mutation on the same chromosome (see section ‘molecular biology’). Therefore we used hetero-allelic combinations in all experiments. For *hisCl1* rescue experiments we used *UAS-hisCl1* (2<sup>nd</sup>, su(Hw)attp5, see below). For RNAi knockdown experiments we used *UAS-hisCl1-RNAi* (2<sup>nd</sup>, VDRC, 104966) and *UAS-dcr2* (3<sup>rd</sup>, Bloomington Stock Center, 24651). For further information on genotypes refer to Table S1.

**METHOD DETAILS****Two-photon calcium imaging**

Flies were dissected and mounted for the recording of inner photoreceptor terminals in the medulla as described previously (Reiff et al., 2010). Briefly, flies were cold anesthetized and glued to a Plexiglas holder with bee wax (at the dorsal thorax) (Figure 1E). The legs were fixed and the head was inclined downward and fixed with wax. Experimental flies were positioned underneath an aluminum holder that at the same time served as recording chamber. Thorax and head of the flies slightly protruded through a small cutout in a thin aluminum sheet that served as the bottom of the recording chamber. The thorax was then glued with wax to the aluminum sheet. The backside of the head was bathed in saline (103 mM NaCl, 3 mM KCl, 3 mM CaCl<sub>2</sub>, 4 mM MgCl<sub>2</sub>, 26 mM NaHCO<sub>3</sub>,

1 mM NaH<sub>2</sub>PO<sub>4</sub>, 10 mM trehalose, 10 mM glucose, 7 mM sucrose, 5 mM TES). The cuticle at the back of the head was dissected away to expose the optic lobe and brain. The post-ocular air sac was medially cut and carefully moved aside to expose the distal medulla.

We used a custom-built two-photon laser scanning microscope (Reiff et al., 2010) for functional calcium imaging equipped with a 40x, 1.0 NA water immersion objective (IR Achromplan; Zeiss). Fluorescence was excited by two-photon excitation using a mode-locked Ti:Sapphire laser (Tsunami, < 100 fs, 80 MHz, 700–1000 nm) pumped by a 10W Millenia laser (both Spectra Physics). Laser intensity was kept constant during the recordings at typically 5 and maximally 10 mW at the specimen. The donor fluorophore mTurquoise2 of Twitch-2C (Figures 1F and 1G) was selectively excited at 823 nm. The emission of mTurquoise2 and of the acceptor fluorophore cpCitrine174 was recorded simultaneously (100 × 100 pixels / image or 50 × 50 pixels / image) at a rate of 4 – 8 Hz using separate emission filters (BP 485/40; BP 535/30) and GaAsP photomultipliers (H10770PA-40 SEL, Hamamatsu) powered by a Sutter PS-2LV (Sutter, Novato, USA). Visual stimuli were presented during the return period of the x-scanning mirror (fly-back stimulation, see below and (Reiff et al., 2010)).

Up to eight neighboring photoreceptor terminals of the same type were recorded simultaneously per image sequence. Individual sequences were 24 – 50 s, depending on the experiment. Sequences were separated by minimum 40 s of darkness to warrant dark-adaptation of the eyes before the beginning of each recording.

### Visual stimulus presentation

Visual stimuli were presented to a large frontal region of the fly's eye. Light from five spectrally different LEDs with maximum emission (in nm) at 517/Green (APG2C1-515), 470/Cyan (APG2C1-470), 430/Blue (APG2C1-435), 375/UV<sub>long</sub> (APG2C1-375-E) and 369/UV<sub>short</sub> (APG2C1-365-E; Roithner Lasertechnik, Vienna, Austria) was focused on individual small light guides (105 μm core diameter, SFS105/125Y, Thorlabs, Newton, USA) that were combined into a single light guide (800 μm core diameter, FT800UMT, Thorlabs, Newton, USA) that was mounted at 1 mm in front of the fly's eye (Figure 1E). Emission of the green and cyan LEDs was short-pass filtered using FF01-533/SP (Semrock, Rochester, USA) optical filters. Python 2.7 software and pulse-width-modulation were used to control the timing and intensity of the LEDs over a range of four magnitudes (10°–10<sup>3</sup> a.u.). The individual LEDs were calibrated for equal quanta flux at each intensity tested (highest intensity (10<sup>3</sup> a.u.) is 3.88 μmol s<sup>-1</sup> m<sup>-2</sup>). A software generated TTL signal at the beginning of each line-scan of the horizontal scanning mirror (x-mirror) of the 2PLSM was generated every 2.5 ms and used to trigger the LED controller. LEDs were OFF during each 1.5 ms line scan (time period used for fluorescence excitation and recording) and switched ON for somewhat less than 1 ms during the time period used to return the x-scanning mirror into its starting position (Figure 1E, fly-back stimulation, (Reiff et al., 2010)). The temporal switching between fluorescence recording and stimulus presentation at a rate of ~400 Hz, which is well above the flicker-fusion frequency of the *Drosophila* eye, prohibited that photons from the wavelength-varying visual stimuli entered the detection pathway of the microscope.

For the analysis of spectral sensitivity, sequences (2 s light ON / 2 s light OFF) of equiluminant visual stimuli were generated using the five different LEDs. Color opponency was investigated by alternatingly presenting preferred monochromatic stimuli (R8y/green, R7y/UV<sub>long</sub>, R8p/blue, and R7p/UV<sub>short</sub>; intensity 10<sup>1</sup> a.u., 2 s) and spectrally composite stimuli. Each stimulus was followed by 2 s darkness. The composite stimuli contained the preferred plus individual other wavelengths, the latter typically presented with higher intensity (10<sup>2</sup> a.u. for analysis of R8p/R8y, and 10<sup>3</sup> a.u. for analysis of R7p/R7y) to facilitate the detection of spectral inhibition. Whether the added second wavelength causes inhibition or additional excitation was analyzed by subtracting the response to the preferred stimulus from the response to the preceding composite stimulus. To analyze the intensity dependence of the inhibitory effect of a given wavelength, we presented a sequence of preferred monochromatic stimuli (with respect to the recorded photoreceptor type, intensity 10<sup>1</sup> a.u., 2 s, followed by 2 s darkness). To every second light pulse a second wavelength was added with variable intensity (Figures S1M–S1P, half-logarithmic increase from 10<sup>1</sup> to 10<sup>3</sup> a.u.).

### Molecular biology and generation of transgenic flies

*UAS-twitch-2C*, *LexAop-twitch-2C*, *rh3(4,5,6)-LexA*, *UAS-CD4-spGFP1-10*, *LexAop-CD4-spGFP11*, and *UAS-hisCl1* genetic constructs were generated by standard procedures. For *UAS-twitch-2C* DNA encoding Twitch-2C (Thestrup et al., 2014) was isolated from pRSSETB by EcoRI/NotI digestion and cloned into pUAST. A BamHI-fragment including Twitch-2C, SV40, 5xUAS and the HsP70 promoter was transferred into pCa4B2G. For *LexAop-twitch-2c* a NotI/XbaI fragment including Twitch-2C DNA was isolated from pUAST-Twitch-2c (see above) and cloned into pJFRC19-13XLexAop2-IVS-myR::GFP (kindly provided by Gerald Rubin, Addgene plasmid #26224) by exchanging myR::GFP. *rh3*, *rh4*, promoter regions were amplified by standard PCR from pCaST-rh3/4-norpA plasmids (kindly provided by Chi-Hon Lee) adding 5'-end AatII- and 3'-end NgoMIV-restriction sites. The resulting AatII/NgoMIV fragment was cloned into pBPnLsLexA::GADfluw (kindly provided by Gerald Rubin, Addgene plasmid #26232). The *rh5* and *rh6* promoter regions were isolated by XbaI digestion of the pCaST-rh5/6-norpA plasmids and a Klenow fragment was inserted into pBPnLsLexA::GADfluw by blunt end ligation.

For *UAS-CD4-spGFP1-10* and *LexAop-CD4-spGFP11* plasmid generation, PCR fragments of GFP1-10 and GFP11 were amplified by standard PCR from gDNA of either *w-;Bl/cyo;UAS-CD4::spGFP1-10/TM2* or *w-;LexAop-CD4::spGFP11/cyo:TM2/TM6B* fly strains (Gordon and Scott, 2009), adding 5'-end XbaI- and 3'-end XbaI-restriction sites. The resulting XbaI/XbaI fragments were cloned into either pJFRC2-10xUAS-IVS-mCD8::GFP, for GFP1-10 or pJFRC19-13X LexAop2-IVS -myR::GFP for GFP11 (see above) by replacing the existing coding sequences. For *UAS-hisCl1* plasmid generation, a PCR fragment of *hisCl1* was amplified by standard

PCR from cDNA preparation (Invitrogen) of Canton S flies (5 heads), adding 5'-end Xhol- and 3'-end XbaI-restriction sites. The resulting Xhol/XbaI fragment was cloned into pJFRC2-10xUAS-IVS-mCD8::GFP (see above) by replacing the mCD8::GFP sequence. All constructs were verified by restriction analysis and sequencing.

Transgenic flies were generated by phiC31-mediated germline transfection in  $y^1v^1P\{nos\text{-}phiC31int.NLS\}X; P\{CarryP\}attP40$  (Bloomington Stock Center, 25709),  $y^1w^*P\{nos\text{-}phiC31int.NLS\}X; PBac\{y^+\text{-}attP\text{-}9A\}VK00027$  (Bloomington Stock Center, 35569),  $y^1w^{1118}P\{nos\text{-}phiC31int.NLS\}X; PBac\{y^+\text{-}attP\}VK00005$  (kindly provided by Hugo Bellen) or  $y^1w^*P\{nos\text{-}phiC31int.NLS\}X; P\{CaryIP\}su(Hw)attP5$  (Bloomington Stock Center, 32231).

All fly stocks used in our recording experiments were tested for *rh6*<sup>1</sup> by analyzing genomic DNA. This 19 bp deletion represents a null-allele that has been observed frequently in common fly stocks. PCR amplifications were done on isolated DNA from five *Drosophila* heads using 5'-tcg gct gga atc ggt atg tg-3' and 5'-tga tct cga tgg cct tgc tc-3' as forward and reverse primers, respectively. PCR products were sequenced and compared to the reference sequences.

### Verification of targeted *hisCl1* expression

We verified the targeted expression of *hisCl1* from our UAS-*hisCl1* genetic construct and fly strain using semiquantitative RT-PCR of *hisCl1* mRNA. *HisCl1* cDNA was prepared from RNA preparations (Invitrogen) from five heads of  $+/UAS\text{-}hisCl1; hisCl1^{384}$  flies, *rh5-GAL4/UAS-hisCl1; hisCl1<sup>384</sup>* flies and wild-type Canton-S flies. Analysis of actin mRNA was used as control. In short: Total RNA was extracted according to the Manufacturer's instructions (Ambion) followed by reverse transcription (RT) which was carried out in a 20  $\mu$ L reaction according to the Manufacturer's instructions (Invitrogen) using the SuperScript III First-Strand Synthesis System. Random hexamers were used as primers for RT. 2  $\mu$ L of the resulting cDNA was used as a template for each of the subsequent PCR reactions.

### Immunohistochemistry

Brains were dissected in PBS and fixed in 4% PFA with 0.1% TritonX for 25 min at room temperature. Brains were subsequently washed four times in 0.5% PBT. The fixed brains were incubated first with PBT-NGS (3% Normal Goat Serum in PBT) for 60 min at 25°C and then with primary antibodies in PBT-NGS at 4°C overnight. The primary antibodies used were rabbit anti-GFP (1:1000, a290, Abcam), mouse anti-GFP (1:100, #G6539, Sigma), rabbit anti-CD4 antibody (1:150, HPA004252, Sigma), rat anti-CadN (1:50, DN-Ex #8, DSHB), and mouse anti-dlg (1:30, 4F3, DSHB). After several washes with PBT, brains were incubated with secondary antibodies in PBT-NGS at 4°C overnight. The secondary antibodies were goat anti-rabbit Alexa Fluor 488 (1:500, A-11008, Life Technologies), anti-mouse Alexa Fluor 488 (1:200, A-11001, Life Technologies), goat anti-rabbit Alexa Fluor 555 (1:200, A-21430, Life Technologies), goat anti-rat Alexa Fluor 405 (1:200, ab175671, Abcam), and goat anti-mouse Alexa Fluor 633 (1:100, A-21053, Life Technologies). After several washes with PBT, brains were mounted (Vectashield, Vector Laboratories) and optically sectioned with a Leica TCS SP8 STED 3X confocal microscope. Fiji software (<http://fiji.sc/>) was used for the processing and analysis of recorded image stacks.

### 3D rendering of R7/R8 photoreceptor EM-reconstructions

EM-reconstructions from (Takemura et al., 2013) were downloaded from <http://neuromorpho.org/> (Ascoli et al., 2007). SWC neuron files were visualized using SharkViewer (<https://github.com/JaneliaSciComp/SharkViewer>; Janelia Research Campus, HHMI).

## QUANTIFICATION AND STATISTICAL ANALYSIS

### Calcium imaging

In the image sequences, potential lateral motion of recorded terminals was routinely compensated using image stabilization software. ROIs were defined by eye based on raw fluorescence images. Fractional changes of the fluorescence ratio  $\Delta R/R$  were calculated after subtracting the raw intensities (multiplied by 0.8) of the background in each of the two simultaneously recorded image sequences over time (t). The instantaneous fluorescence ratio  $R_t = (\text{acceptor} - 0.8 \cdot \text{background}_{\text{acceptor}})_t / (\text{donor} - 0.8 \cdot \text{background}_{\text{donor}})_t$  and  $\Delta R/R [\%] = ((R_t - R_0) / R_0) \times 100\%$  was calculated with  $R_0$  being the average of the first 5–12 images before stimulus onset. Bleach in the obtained  $\Delta R/R$  time courses was corrected using single exponential decay functions.  $\Delta R/R$  maximum responses to each stimulus were derived by calculating the median  $\Delta R/R$  during the last second of each stimulus period. Imaging data was analyzed using MBF-ImageJ (US National Institutes of Health) and Python 2.7 software.

### Statistics

Statistical analysis was performed using SciPy (<https://www.scipy.org/>) and Python 2.7 software. All sample sizes were large enough for robust statistical tests. Groups that fulfilled the assumption of normal distribution (Shapiro-Wilk test) were tested for significant differences from zero using one-sample t tests. Otherwise, the nonparametric Wilcoxon signed-rank test was used. Prior to comparison of groups, both Shapiro-Wilk test for normal distribution and Levene test for equality of variances were applied. Groups not significantly different from normal distribution and with similar variances were analyzed by one-way ANOVA followed by post hoc pairwise one-sample t tests. Otherwise, the non-parametric Kruskall-Wallis H test was performed, followed by post hoc pairwise

Mann-Whitney-U tests. *P* values of all tests were corrected according to the Holm-Bonferroni method to control for the false discovery rate within multiple comparisons. Statistical details of experiments can be found in the figure legends. We report number of recordings in single photoreceptor terminals (*n*) and number of animals [enclosed in square brackets] in which recordings were performed in Table S1. Since most data was not distributed normally, we plotted the median, 10 / 90%, and 25 / 75% quantiles to visualize data.

#### DATA AND SOFTWARE AVAILABILITY

Raw data and analysis code will be provided upon request by Lead Contact, Dierk F. Reiff ([dierk.reiff@biologie.uni-freiburg.de](mailto:dierk.reiff@biologie.uni-freiburg.de)).

# Supplemental Figures

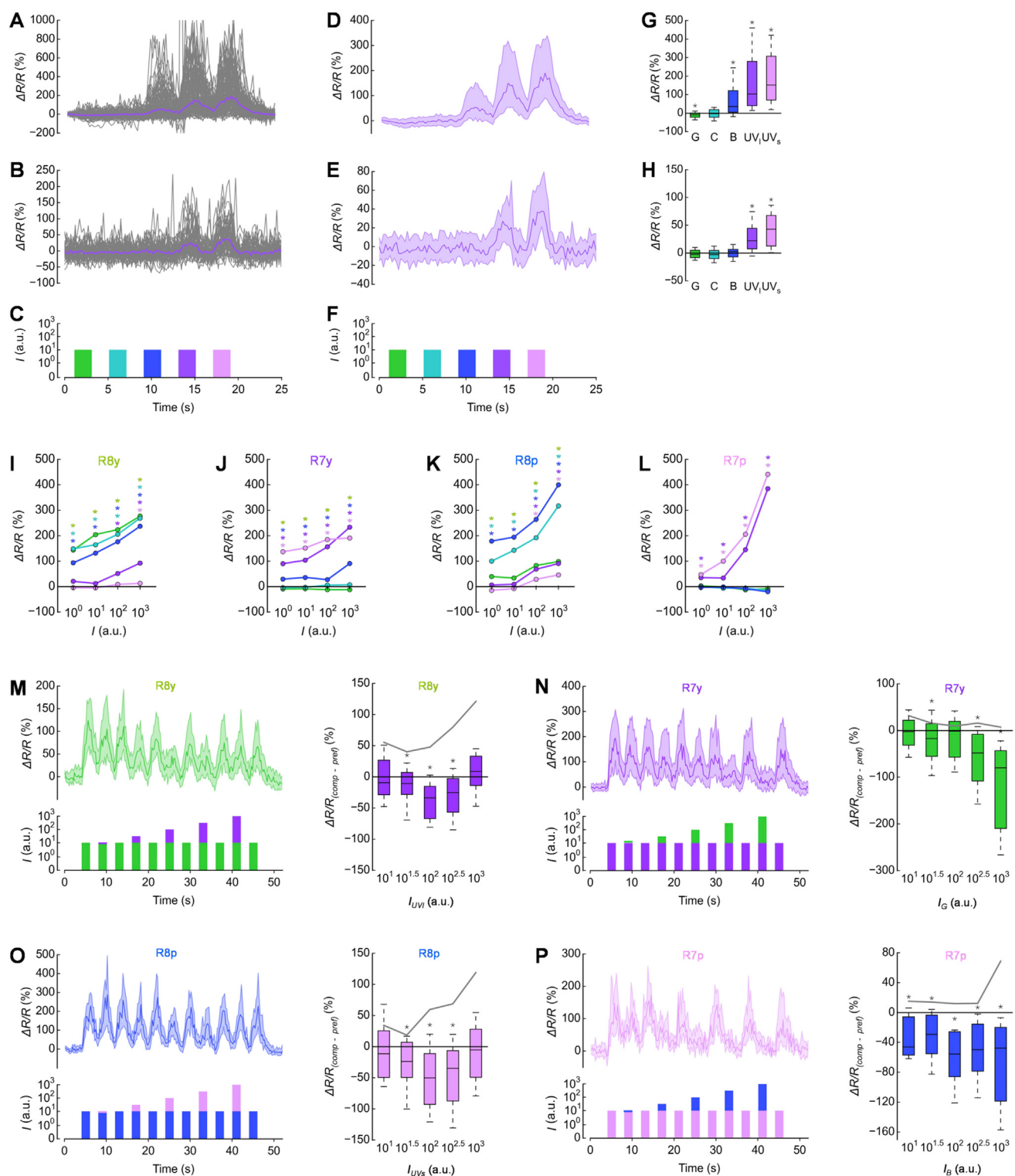


**Figure S1. Comparison of Twitch-2C and TN-XL Fluorescence Changes and Responses to Monochromatic and Composite Stimuli of Varying Intensities in Inner Photoreceptor Terminals, Related to Figures 2–4**

(A–C) Individual recording traces (gray) and median trace (purple) of  $\Delta R/R$  fluorescence changes in (A) Twitch-2C (Thestrup et al., 2014) and (B) TN-XL (Mank et al., 2006) expressing R7y terminals during the presentation of (C) monochromatic visual stimuli (intensity  $10^1$  a.u.). Twitch-2C with a  $K_d = 450$  nM *in vitro* exhibited larger responses than TN-XL with a  $K_d = 2.2 \mu\text{M}$  *in vitro* (Mank et al., 2006). In R7y, the *in vivo* decay time of the fluorescence signal of Twitch-2C ( $\tau_{\text{decay}} = 1.31$  s)

(legend continued on next page)

was shorter than *in vitro* ( $\tau_{\text{decay}} = 2.6$  s) (Thestrup et al., 2014). However, when compared to Twitch-2C, the decay time of the TN-XL fluorescence in R7y was much shorter ( $\tau_{\text{decay}} = 0.40$  s). The experiments using TN-XL suggest that intracellular calcium in inner photoreceptor terminals decreases very rapidly to baseline after the visual stimulus is shut off. The slow decay visible in our recordings using Twitch-2C can most likely be attributed to the slow OFF-rate of the calcium reporter Twitch-2C, and was not caused by the calcium dynamics of photoreceptor terminals.

(D–F) Same data as in (A) and (B), median traces and 25% and 75% quantiles. (D) Twitch-2C and (E) TN-XL-expressing R7y terminals during the presentation of (F) monochromatic visual stimuli.

(G and H) Maximum fractional changes of the fluorescence ratio  $\Delta R/R$  in (A) and (B). Significant inhibition to green and excitation to blue light was detected with (G) Twitch-2C but not (H) TN-XL. Same type of plots as in Figure 2.

(I–L) Maximum responses in Twitch-2C expressing inner photoreceptor terminals (I) R8y, (J) R7y, (K) R8p, and (L) R7p to different monochromatic light pulses presented at four different intensities ( $10^0$  –  $10^3$  a.u.; otherwise same stimulus protocol as in Figure 2C). Light of all used intensities did not elicit obvious saturation of the fluorescence response in any of the photoreceptor terminals, including intensities that approximated the intensity of composite stimuli in Figure 3. Data points represent the median, color indicates the color of the presented visual stimuli (green = green stimuli; cyan = cyan stimuli; blue = blue stimuli; dark purple = UV<sub>long</sub> stimuli; light purple = UV<sub>short</sub> stimuli, see Figure 1). Asterisks indicate responses significantly different from R<sub>0</sub> ( $p < 0.05$ ; Wilcoxon test).

(M) Time course of fluorescence changes and maximum responses of R8y terminals to preferred green stimuli (intensity  $10^1$  a.u.) and different intensity ratios of green and UV<sub>long</sub> stimuli ( $10^1:10^1$ ,  $10^1:10^{1.5}$ ,  $10^1:10^2$ ,  $10^1:10^{2.5}$ ,  $10^1:10^3$  a.u.; stimulus protocol depicted below the recording traces). Left: Time course of the fluorescence change  $\Delta R/R$ . Right: Comparison of responses to green and composite stimuli ( $\Delta R/R_{\text{comp}} - \Delta R/R_{\text{pref}}$ ). Additive and spectrally opponent processing of the composite stimuli is indicated by positive and negative values, respectively. Spectral inhibition was observed for ratios of green and UV<sub>long</sub> stimuli of  $10^1:10^{1.5}$ ,  $10^1:10^2$ , and  $10^1:10^{2.5}$  a.u.

(N) Same experiment as in (A) but recording in R7y terminals with UV<sub>long</sub> as preferred stimulus and different intensity ratios of UV<sub>long</sub> and green stimuli. Spectral inhibition was observed for ratios of  $10^1:10^{1.5}$ ,  $10^1:10^{2.5}$ , and  $10^1:10^3$  a.u.

(O) Same experiment as in (A) but recording in R8p terminals with blue as preferred stimulus and different intensity ratios of blue and UV<sub>short</sub> stimuli. Spectral inhibition was observed for ratios of  $10^1:10^{1.5}$ ,  $10^1:10^2$ , and  $10^1:10^{2.5}$  a.u.

(P) Same experiment as in (A) but recording in R7p terminals with UV<sub>short</sub> as preferred stimulus and different intensity ratios of UV<sub>short</sub> and blue stimuli. Spectral inhibition was observed for all tested ratios.

Recording traces and boxplots in (M–P) as in Figure 3. Asterisks indicate significant inhibition or additional excitation ( $p < 0.05$ ; Wilcoxon test). The gray line in the boxplots to the right indicates median responses recorded in flies with functional phototransduction in only the recorded type of photoreceptor (photoreceptor-specific *norpA* rescue, see Figure 4, Figures S2, S3, S4, and S5, and Table S1).

For exact genotypes and  $n$  recordings see Table S1.

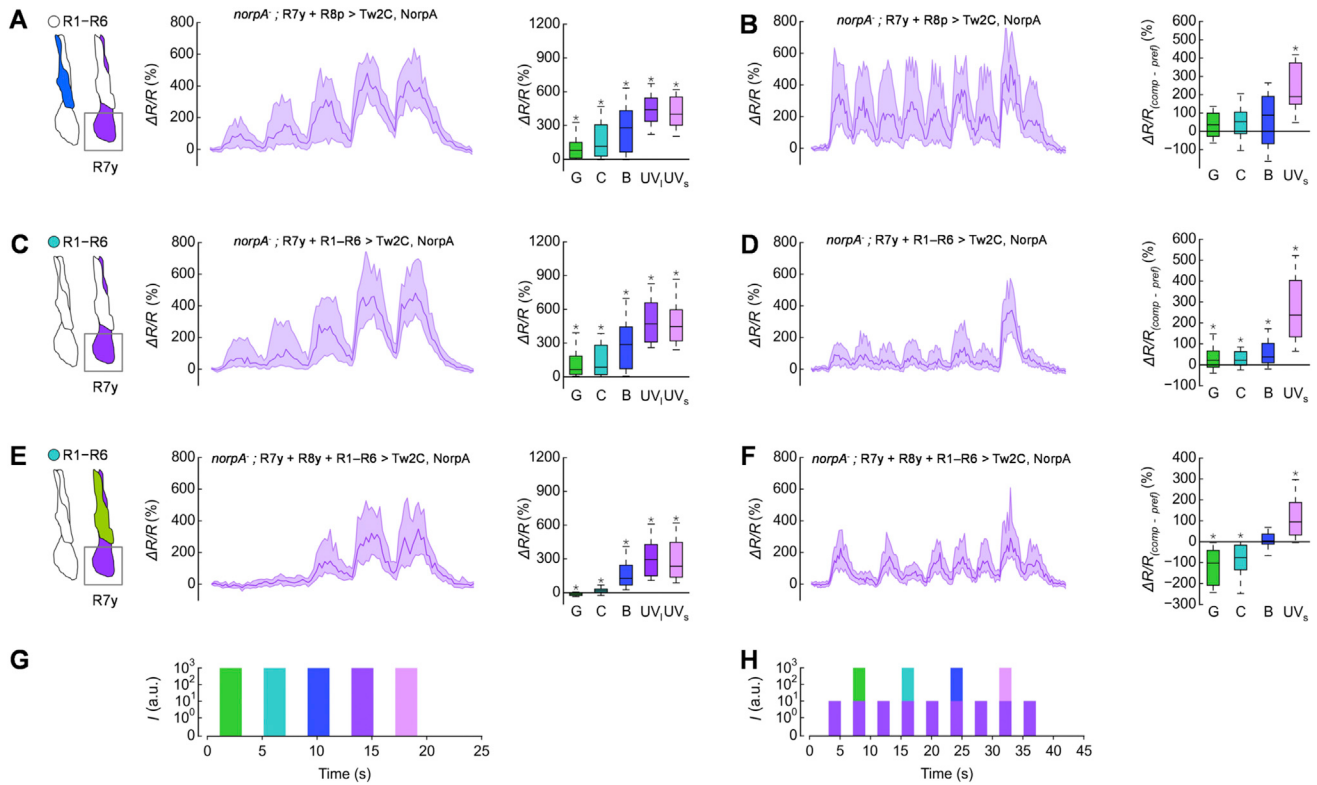


**Figure S2. Spectral Tuning and Opponent Processing Are Not Restored in R7y Terminals When Functional R7y Photoreceptors Are Combined with Functional Photoreceptors Other Than R8y, Related to Figure 4**

(A) Time course of fluorescence changes (purple trace) and maximum responses (boxplots) of R7y terminals in response to monochromatic stimuli (intensity  $10^3$  a.u., see G) in flies with light sensitivity in only R7y and R8p (*norpA* mutant flies, *norpA* rescue in R7y and R8p). R7y terminals showed excitatory responses at all wavelengths tested including green ( $p < 0.05$ ; Wilcoxon test), similar to the responses of R7y terminals if only R7y was functional (Figure 4A). In control flies, R7y terminals were slightly but significantly inhibited by green light (Figure S1J and black trace in Figure 4A;  $p < 0.05$ ; Wilcoxon test).

(B) Time course of fluorescence changes and comparison of responses to preferred monochromatic ( $UV_{long}$ ) and composite stimuli (H) in R7y terminals in same *norpA* rescue flies as in (A). R7y responses to  $UV_{long}$  were not antagonized by green and cyan light ( $p > 0.05$ ; one-sample t test), similar to flies with function in only R7y (Figure 4B). In R7y terminals of control flies, spectral inhibition was observed when green or cyan light was added to  $UV_{long}$  ( $p < 0.05$ ; Wilcoxon test; Figures 3B and 3F).

(C and D) Same experiment as in (A and B) but *norpA* rescue in R7y and R1-R6 cells. Additional function in R1-R6 photoreceptors neither restored (C) spectral tuning (excitatory response to green and cyan light;  $p < 0.05$ ; Wilcoxon test) nor (D) color-opponent processing in R7y terminals (additive processing when green or cyan light was added to  $UV_{long}$ ;  $p < 0.05$ ; Wilcoxon test). These results are qualitatively similar to *norpA* rescue in only R7y in Figure 4B.

(E and F) Same experiment as in (A and B), but *norpA* rescue in R1-R6, R7y and R8y cells. In these flies the responses of R7y terminals resembled those of R7y terminals in flies with functional R7y/R8y cells (Figures 4C and 4D). (E) Inhibitory response to green light ( $p < 0.05$ ; Wilcoxon test) and (F) spectral inhibition were rescued when green or cyan light was added to  $UV_{long}$  ( $p < 0.05$ ; Wilcoxon test).

Functional photoreceptors are depicted in color in the schemes at left. Same type of plots as in Figures 2 and 3, asterisks indicate responses significantly different from R<sub>0</sub> in (A, C, E) and significant inhibition or additional excitation in (B, D, F) ( $p < 0.05$ ; Wilcoxon or one-sample t test).

For exact genotypes and  $n$  recordings see Table S1.

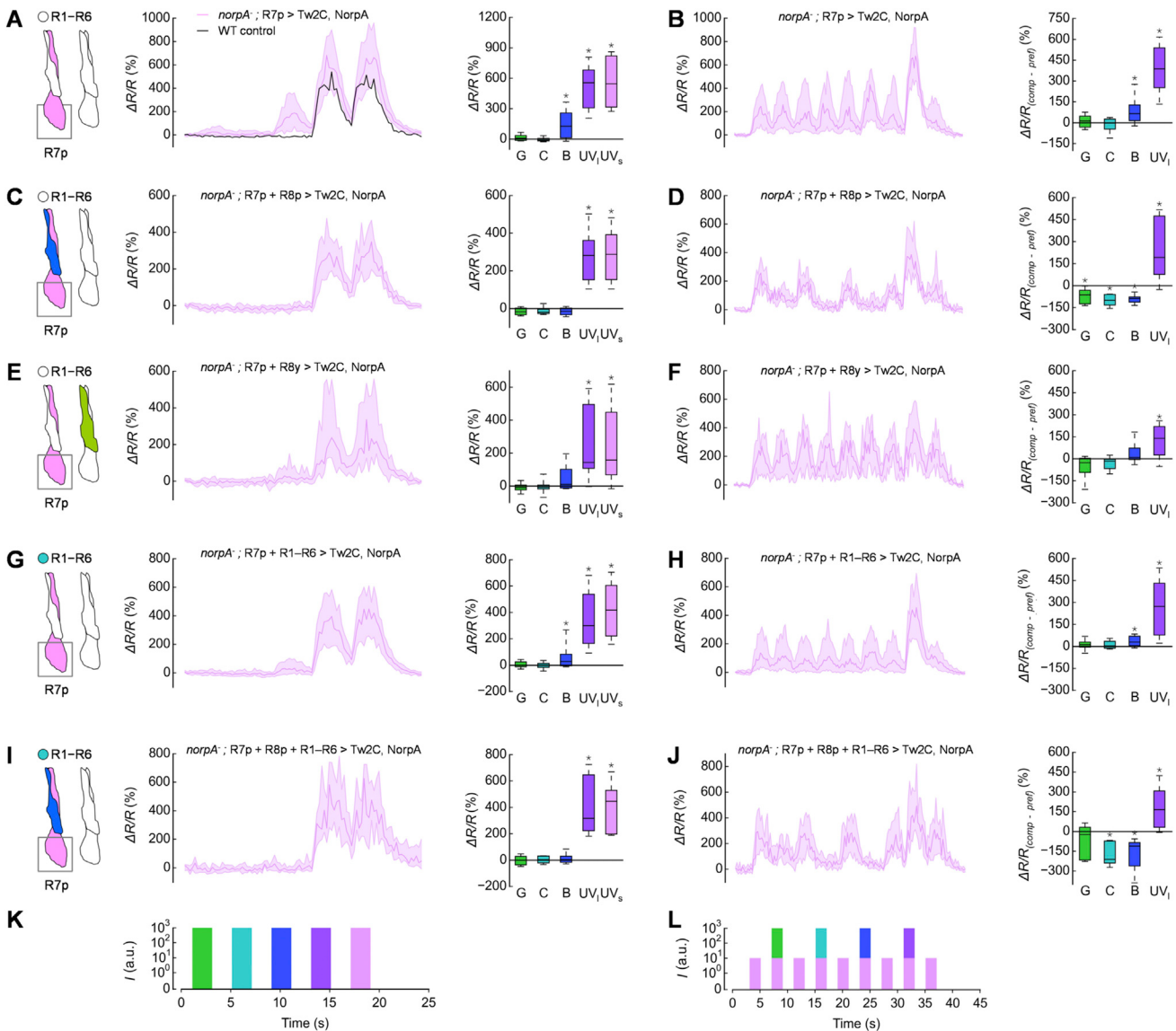


**Figure S3. Spectral Tuning and Opponent Processing in R7p Terminals Require Intact Function in R7p and R8p Cells, Related to Figure 4**

(A) Time course of fluorescence changes (purple trace) and maximum responses (boxplots) of R7p terminals in response to monochromatic stimuli (intensity  $10^3$  a.u., see K) in flies with light sensitivity in only R7p photoreceptors (*norpA* mutant with *norpA* rescue in R7p). In addition to UV, R7p of these flies were excited by blue light (light purple trace;  $p < 0.05$ ; Wilcoxon test; black trace shows responses of R7p terminals in control flies with intact phototransduction in all photoreceptors, see also Figure S1L).

(B) Time course of fluorescence changes and comparison of responses to preferred monochromatic ( $UV_{short}$ ) and composite stimuli (L) in R7p terminals in same *norpA* rescue flies as in (A). Responses of R7p terminals to  $UV_{short}$  were not antagonized by green and cyan light ( $p > 0.05$ ; one-sample t test).  $UV_{short}$  plus blue light was processed additively ( $p < 0.05$ ; one-sample t test). In R7p terminals of control flies, additive processing was only observed when both UV stimuli were combined (Figures 3D and 3H), which was similarly observed in the here analyzed mutant flies ( $p < 0.05$ ; one-sample t test).

(C and D) Same experiments as in (A and B) but *norpA* rescue in R7p/R8p cells. Intact function in R7p/R8p photoreceptors (C) restored spectral tuning of R7p terminals (no sensitivity for blue,  $p > 0.05$ ; Wilcoxon test), and (D) restored color-opponent processing in R7p terminals. Responses to  $UV_{short}$  stimuli were antagonized by simultaneous green, cyan or blue stimuli (spectral inhibition;  $p < 0.05$ ; one-sample t test).

(E and F) Same experiments as in (A and B) but *norpA* rescue in R7p/R8y photoreceptors. (E) R7p terminals exhibited excitatory responses only to the UV stimuli ( $p < 0.05$ ; Wilcoxon test). (F) Intact function in R7p/R8y did not restore color-opponent processing in R7p. Addition of green, cyan or blue to  $UV_{short}$  stimuli did not elicit significant inhibition in R7p terminals ( $p > 0.05$ ; Wilcoxon test).

(G and H) Same experiments as in (A and B) but *norpA* rescue in R7p and R1-R6 photoreceptors. Additional function in R1-R6 neither restored (G) spectral tuning (response to blue light;  $p < 0.05$ ; Wilcoxon test) nor (H) color-opponent processing in R7p terminals (additive processing with blue light;  $p < 0.05$ ). Results are qualitatively similar to *norpA* rescue in only R7p cells in (A and B).

(legend continued on next page)

(I and J) Same experiments as in (A and B), but *norpA* rescue in R1–R6, R7p and R8p cells. In these flies, the responses of R7p terminals resembled those of R7p in flies with functional phototransduction in R7p and R8p (C and D), and in flies with unperturbed visual circuits (black trace in A): (I) no response to blue light ( $p > 0.05$ ; Wilcoxon test), (J) spectral inhibition when cyan or blue was added to UV<sub>short</sub> light ( $p < 0.05$ ; Wilcoxon test). Functional photoreceptors are depicted in color in the schemes at left. Same type of plots as in Figures 2 and 3, asterisks indicate responses significantly different from  $R_0$  in (A, C, E, G, I) and significant inhibition or additional excitation in (B, D, F, H, J) ( $p < 0.05$ ; Wilcoxon or one-sample t test). For exact genotypes and  $n$  recordings see Table S1.

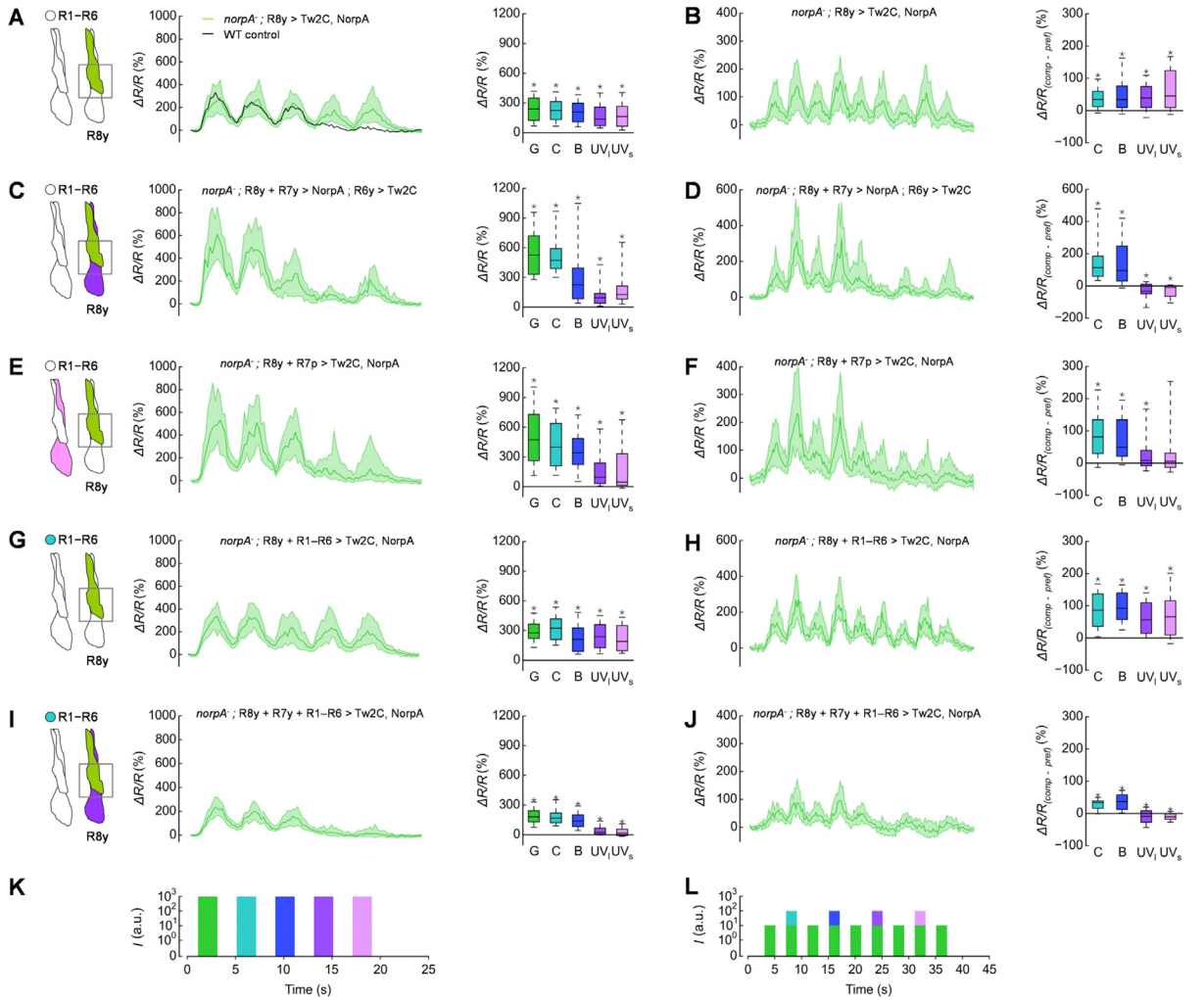


**Figure S4. Spectral Tuning and Opponent Processing in R8y Terminals Require Intact Function in R8y and R7y Cells, Related to Figure 4**

(A) Time course of fluorescence changes (green trace) and maximum responses (boxplots) of R8y terminals in response to monochromatic stimuli (intensity  $10^3$  a.u., see K) in flies with light sensitivity in only R8y photoreceptors (*norpA* mutant with *norpA* rescue in R8y cells). In these flies, R8y terminals exhibited large responses to green, cyan, blue and both UV stimuli (green trace;  $p < 0.05$ ; Wilcoxon test). R8y terminals of control flies exhibited comparable responses to green, cyan and blue stimuli but only small (yet significant) responses to the UV stimuli (black trace,  $p < 0.05$ ; Wilcoxon test. See Figure S1).

(B) Time course of fluorescence changes and comparison of responses to preferred monochromatic (green) and composite stimuli (L) in R8y terminals in same *norpA* rescue flies as in (A). Responses of R8y terminals to green light were not antagonized by UV light ( $p < 0.05$ ; one-sample t test), instead green plus each of the individual other stimuli were processed additively ( $p < 0.05$ ; Wilcoxon test. Compare with control in Figures 3A and 3E).

(C and D) Same experiments as in (A and B) but *norpA* rescue in R7y/R8y cells. Intact function in R7y/R8y photoreceptors (C) restored the spectral tuning of R8y terminals (both UV stimuli elicited only small responses in R8y terminals;  $p < 0.05$ ; Wilcoxon test), and (D) restored color-opponent processing in R8y terminals. Responses to green are antagonized by simultaneous UV light (spectral inhibition;  $p < 0.05$ ; Wilcoxon test).

(E and F) Same experiments as in (A and B) but *norpA* rescue in R7p/R8y cells. (E) All monochromatic stimuli elicited significant excitatory responses in R8y terminals ( $p < 0.05$ ; Wilcoxon test). Although these responses are comparable to the responses in (C), the antagonistic processing of spectrally composite stimuli was not restored (F). Addition of the UV stimuli to green light did not elicit significant inhibition ( $UV_{long}$ ,  $p < 0.05$ , indicating additive processing;  $UV_{short}$ ,  $p > 0.05$ ; Wilcoxon test).

(G and H) Same experiments as in (A and B) but *norpA* rescue in R8y and R1-R6 cells. Additional function in R1-R6 photoreceptors neither restored (G) spectral tuning (large responses to UV light;  $p < 0.05$ ; Wilcoxon test) nor (H) color-opponent processing in R8y terminals (additive processing with UV light;  $p < 0.05$ ; Wilcoxon test). These results are qualitatively similar to *norpA* rescue in only R8y in (A and B).

(I and J) Same experiments as in (A and B), but triple *norpA* rescue in R1-R6, R7y and R8y cells. In these flies the terminals of R8y responded qualitatively similar to those of R8y terminals in flies with function in exclusively R7y/R8y photoreceptors (C and D) and in flies with unperturbed circuits (black trace in A): (I) small responses to UV light ( $p < 0.05$ ; Wilcoxon test), (J) spectral inhibition when mixing either of the two UV stimuli with green light ( $p < 0.05$ ; t test test). Functional photoreceptors are depicted in color in the schemes at left. Same type of plots as in Figures 2 and 3, asterisks indicate responses significantly different from  $R_0$  in (A, C, E, G, I) and significant inhibition or additional excitation in (B, D, F, H, J) ( $p < 0.05$ ; Wilcoxon or one-sample t test). For exact genotypes and  $n$  recordings see Table S1.

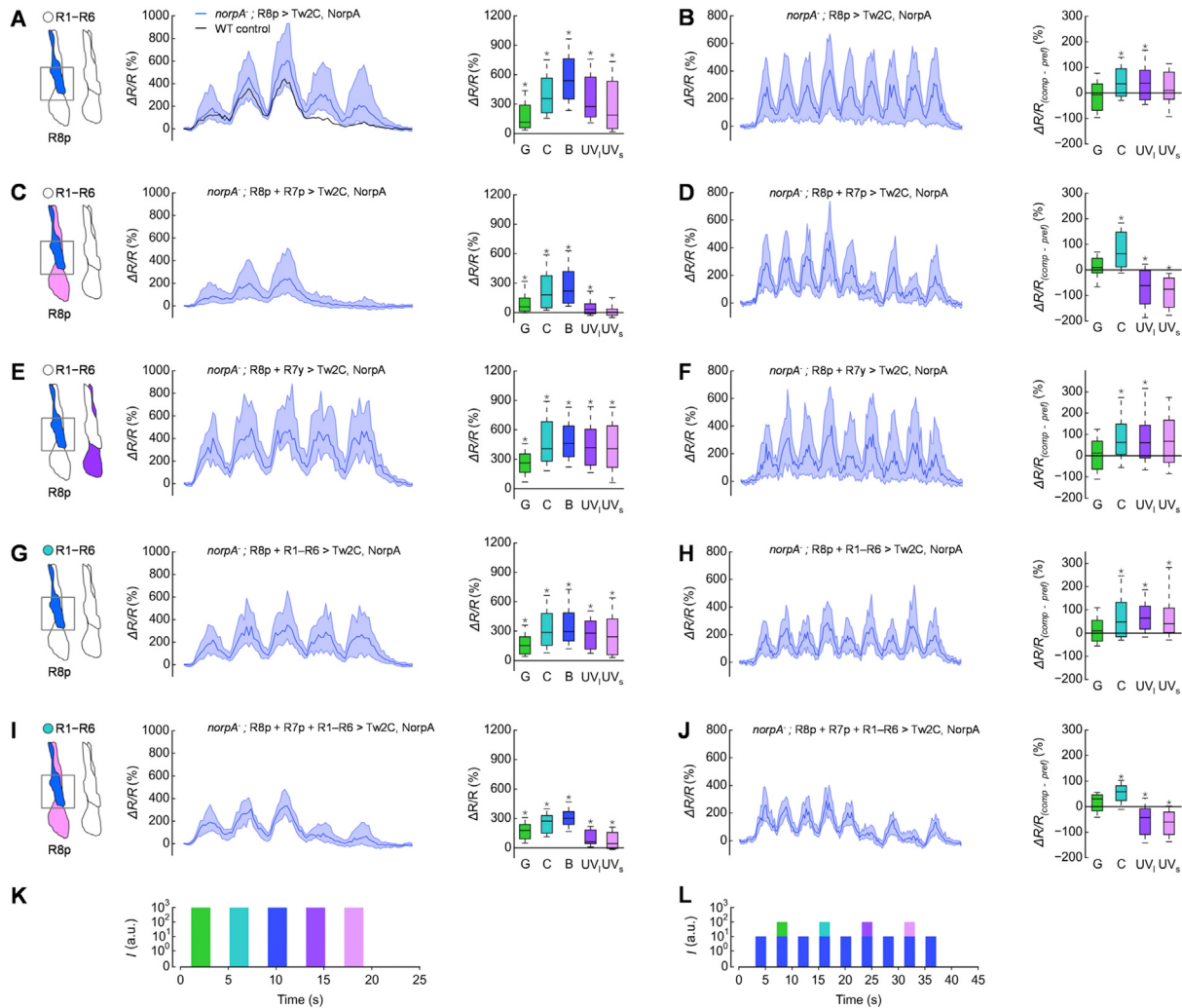


**Figure S5. Spectral Tuning and Opponent Processing in R8p Terminals Require Intact Function in R8p and R7p Cells, Related to Figure 4**

(A) Time course of fluorescence changes (green trace) and maximum responses (boxplots) of R8p terminals in response to monochromatic stimuli (intensity  $10^3$  a.u., see (K)) in flies with light sensitivity in exclusively R8p photoreceptors (*norpA* mutant with *norpA* rescue in R8p cells). R8p terminals exhibited large responses to both UV stimuli and increasingly larger responses to green, cyan and blue stimuli (blue trace;  $p < 0.05$ ; Wilcoxon test). R8p terminals of control flies exhibited comparable responses to the long wavelength stimuli but only small responses to the UV stimuli (black trace,  $p < 0.05$ ; Wilcoxon test. See Figure S1K).

(B) Time course of fluorescence changes and comparison of responses to preferred monochromatic (green) and composite stimuli (L) of R8p terminals in same *norpA* rescue flies as in (A). The responses of R8p terminals to blue were not antagonized by UV<sub>long</sub> (additive processing;  $p < 0.05$ ; Wilcoxon test) or UV<sub>short</sub> light ( $p > 0.05$ ; Wilcoxon test). R8p terminals in control flies were inhibited by both UV stimuli ( $p < 0.05$ ; Wilcoxon test. See Figures 3C and 3G).

(C and D) Same experiments as in (A and B) but *norpA* rescue in R7p/R8p cells. Intact function in R7p/R8p photoreceptors (C) restored the spectral tuning of R8p terminals, i.e., increasing sensitivity to green, cyan and blue and only little sensitivity for UV light (UV<sub>short</sub>:  $p > 0.05$ ; UV<sub>long</sub>:  $p < 0.05$  Wilcoxon test), comparable to control flies, black trace in (A). (D) In these flies color-opponent processing in R8p was restored. Responses to blue were effectively antagonized by simultaneous UV light (spectral inhibition;  $p < 0.05$ ; Wilcoxon test).

(E and F) Same experiments as in (A and B) but *norpA* rescue in R7y/R8p cells. (E) R8p terminals showed large excitatory responses to all stimuli, in particular UV light ( $p < 0.05$ ; Wilcoxon test). (F) Intact function in R7p/R8y photoreceptors did not restore color-opponent processing in R8p terminals. When combined with blue light, neither of the UV stimuli elicited inhibition ( $p > 0.05$ ; Wilcoxon test. Compare with control in Figures 3C and 3G).

(G and H) Same experiments as in (A and B) but *norpA* rescue in R8p and R1-R6 cells. Additional function in R1-R6 photoreceptors neither restored (G) spectral tuning (large responses to UV light;  $p < 0.05$ ; Wilcoxon test) nor (H) color-opponent processing in R8p terminals (additive processing with UV;  $p < 0.05$ ). These results are qualitatively similar to *norpA* rescue in only R8p photoreceptors in (A and B).

(I and J) Same experiments as in (A and B) but *norpA* rescue in R1-R6, R7p and R8p cells. In these flies, the responses of R8p terminals resembled those in R8p in flies with function in only R7p and R8p (C and D) and in flies with unperturbed circuits (black trace in A): (I) small responses to UV light ( $p < 0.05$ ; Wilcoxon test), (J) spectral inhibition when mixing either of the UV stimuli with blue light ( $p < 0.05$ ; Wilcoxon test).

Functional photoreceptors are depicted in color in the schemes at left. Same type of plots as in Figures 2 and 3, asterisks indicate responses significantly different from R<sub>0</sub> in (A, C, E, G, I) and significant inhibition or additional excitation in (B, D, F, H, J) ( $p < 0.05$ ; Wilcoxon test). For exact genotypes and  $n$  recordings see Table S1.

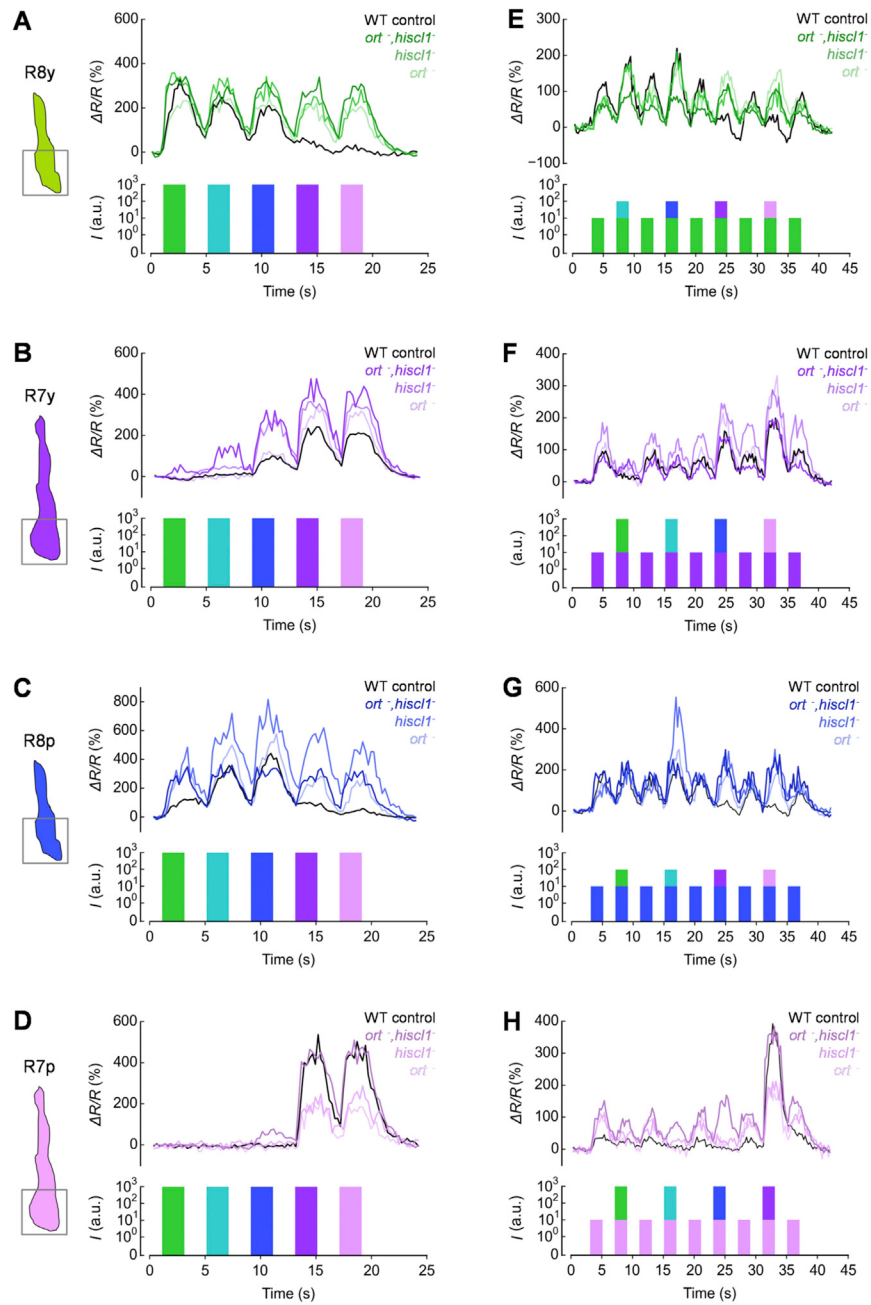


**Figure S6. Ort and HisCl1 Are Differentially Required for Opponent Processing in R7 and R8 Terminals, Related to Figure 6**

(A–D) Time courses of the fluorescence changes in response to monochromatic stimuli in (A) R8y, (B) R7y, (C) R8p, and (D) R7p terminals in control, *ort<sup>+</sup>, hisCl1<sup>-</sup>*, and *ort<sup>+</sup>, hisCl1<sup>-</sup>* mutant flies (intensity 10<sup>3</sup> a.u., stimulus protocol below traces).

(E–H) Time courses of fluorescence changes in response to preferred monochromatic and composite stimuli in photoreceptor terminals of same flies as in (A–D) (stimulus protocol below traces). (E) R8y, (F) R7y, (G) R8p, and (H) R7p terminals.

For quantification of the responses refer to Figure 6. Recording traces represent median. For genotypes and *n* recordings see Table S1.

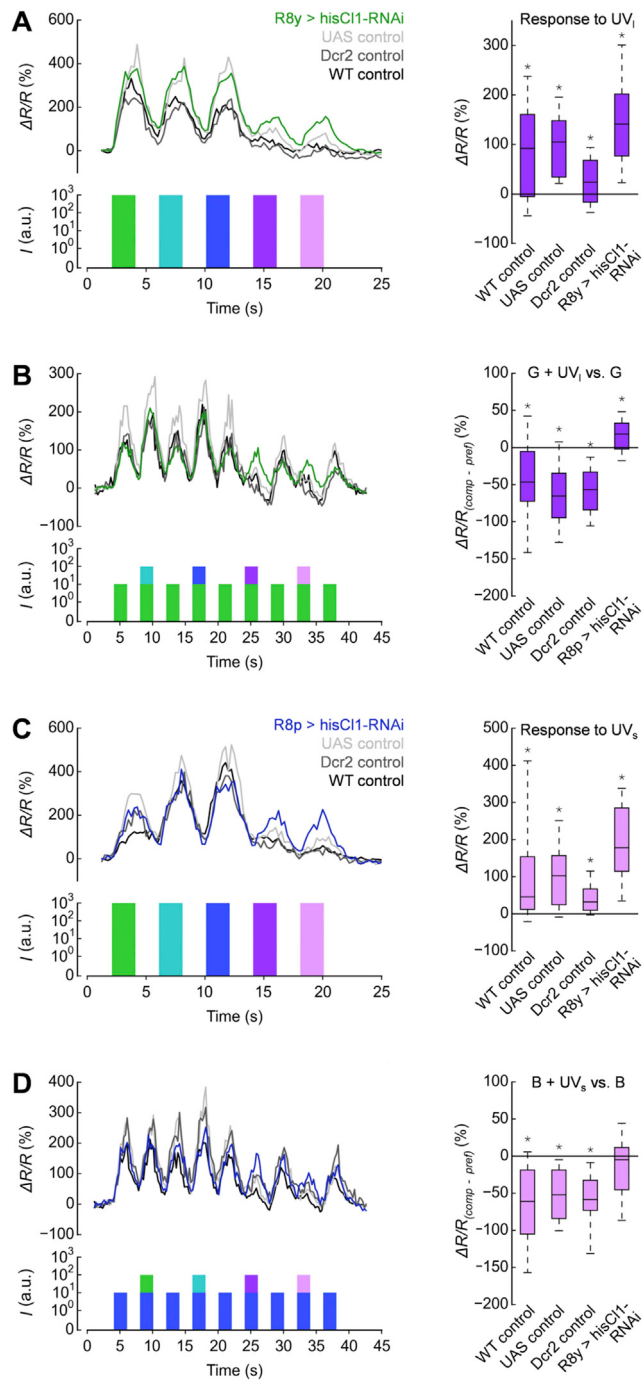


**Figure S7. HisC1 Expression Is Required for Opponent Processing in R8 Cells, Related to Figure 6**

(A) Time course of fluorescence changes and maximum responses to  $UV_{long}$  stimuli in R8y terminals in flies with *hisC1* knockdown in R8y (R8y > *hisC1*-RNAi with coexpression of Dcr2), WT control flies, UAS control flies (harboring *UAS-hisC1-RNAi* and *UAS-dcr2*) and Dcr2 control flies (R8y > *dcr2*) (intensity 10<sup>3</sup> a.u., stimulus protocol below recording traces). R8y terminals with *hisC1* knockdown showed larger response to  $UV_{long}$  stimuli than R8y terminals in all three types of control flies ( $p < 0.05$ , Kruskal-Wallis H test;  $p < 0.05$ , post hoc Mann-Whitney U tests).

(B) Same flies as in (A); time course of fluorescence changes in R8y terminals and comparison of responses to preferred green and composite stimuli that include green and  $UV_{long}$  light. In contrast to R8y terminals in all control flies, R8y terminals with *hisC1* knockdown did not display spectral inhibition and processed composite stimuli additively ( $p < 0.05$ , Wilcoxon test). Furthermore, R8y terminals with *hisC1* knockdown showed larger  $\Delta R/R_{(comp - pref)}$  than R8y terminals in all three types of control flies ( $p < 0.05$ , Kruskal-Wallis H test;  $p < 0.05$ , post hoc Mann-Whitney U tests).

(C and D) Similar experiments as in (A and B) but *hisC1* knockdown in R8p. (C) R8p terminals in *hisC1* KD flies showed larger response to  $UV_{short}$  stimuli than R8p terminals in all three control flies ( $p < 0.05$ , Kruskal-Wallis H test;  $p < 0.05$ , post hoc Mann-Whitney U tests). (D) In contrast to R8y terminals in all types of control

(legend continued on next page)

flies, R8p terminals with *hisC1* knockdown were not spectrally inhibited when UV<sub>short</sub> was added to the blue stimulus ( $p > 0.05$ , Wilcoxon test). Compared to R8p terminals in all types of control flies, R8p terminals in *hisC1* KD flies showed increased  $\Delta R/R_{(comp - pref)}$  ( $p < 0.05$ , Kruskal-Wallis H test;  $p < 0.05$ , post hoc Mann-Whitney U tests).

Recording traces represent median. For exact genotypes and  $n$  recordings see [Table S1](#).

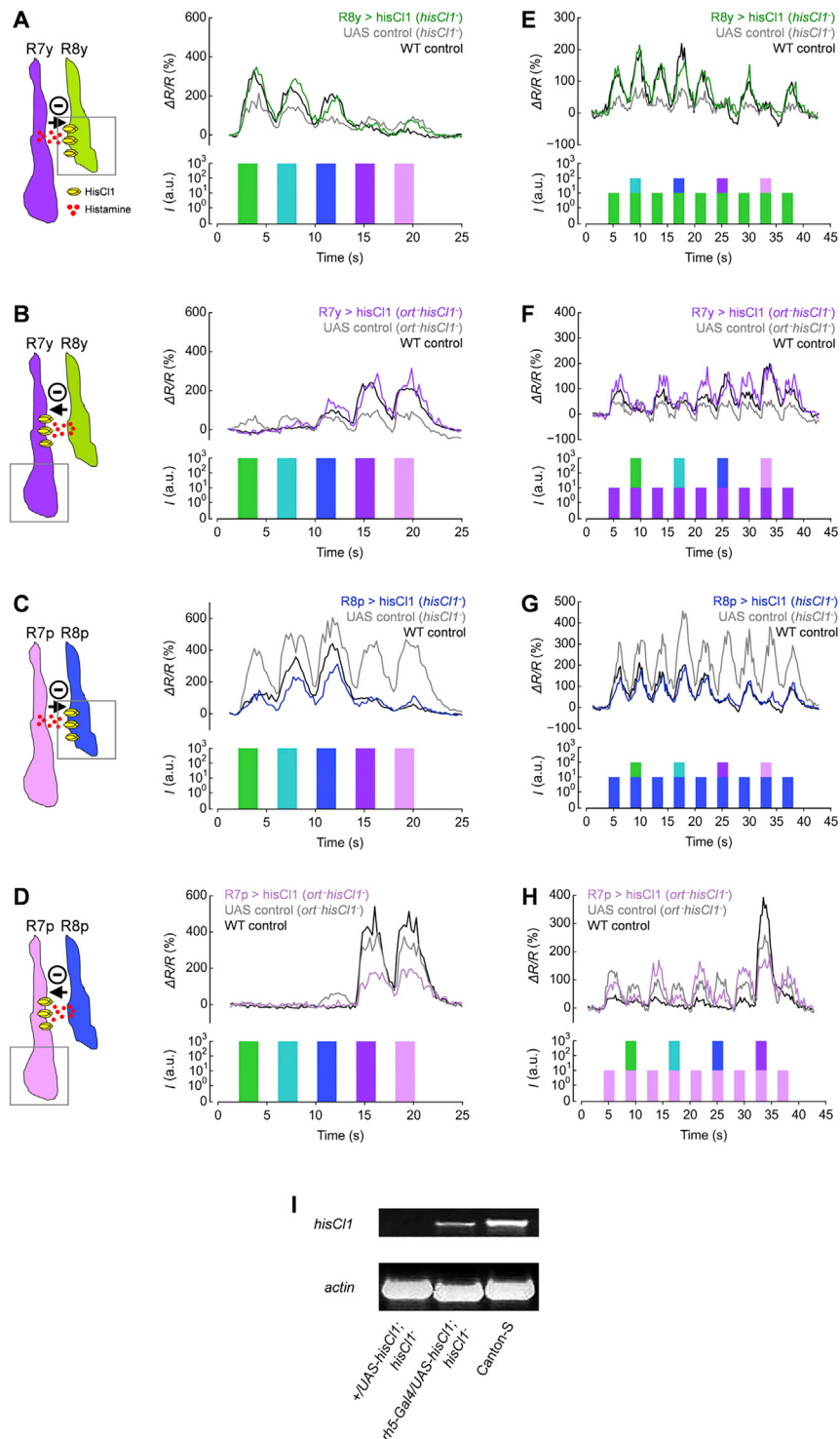


**Figure S8. HisCl1 Rescue in Single Photoreceptor Types Restores Spectral Processing, Related to Figure 7**

(A–D) Time courses of the fluorescence changes to monochromatic stimuli in (A) R8y, (B) R7y, (C) R8p, and (D) R7p terminals (intensity  $10^3$  a.u., stimulus protocol below recording traces). Expression of *hisCl1* was rescued in R8 and R7 in *hisCl1*<sup>-</sup> mutant flies and in *hisCl1*<sup>-</sup>/*ort*<sup>-</sup> double mutant flies, respectively. The different mutant backgrounds were chosen to account for the differential requirement of both histamine receptors for color opponent processing in R7 and R8 (Figure 6). Three different genotypes were analyzed: *hisCl1* rescue flies (*hisCl1*<sup>-</sup> or *hisCl1*<sup>-</sup>/*ort*<sup>-</sup> mutants, harboring *UAS-hisCl1* and GAL4-driver), positive control flies (unperturbed circuits), and negative control flies (*hisCl1*<sup>-</sup> or *hisCl1*<sup>-</sup>/*ort*<sup>-</sup> mutants, harboring *UAS-hisCl1*).

(legend continued on next page)

(E–H) Time courses of fluorescence changes to preferred monochromatic and composite stimuli in same receptor terminals and genotypes as in (A–D) (stimulus protocol below traces). (E) R8y, (F) R7y, (G) R8p, and (H) R7p terminals.

(I) Verification of the generated *UAS-hisCl1* fly line by RT-PCR. *HisCl1* mRNA was detectable in *hisCl1* mutant flies with ectopic *hisCl1* expression in only R8p photoreceptors (middle; *rh5-GAL4/UAS-hisCl1; hisCl1<sup>384</sup>*), and more strongly in wild-type Canton-S flies (right). *HisCl1*mRNA could not be detected in *hisCl1* mutant flies with *UAS-hisCl1* (left, *+/UAS-hisCl1; hisCl1<sup>384</sup>*). *Actin* mRNA was analyzed as control; heads of flies were analyzed.

Recording traces represent median. For quantification of the responses refer to [Figure 7](#). For exact genotypes and  $n$  recordings see [Table S1](#).